JOURNAL OF COMPUTATIONAL PHYSICS 113, 224-248 (1994)

A New Lagrangian Method for Three-Dimensional Steady Supersonic Flows

CHING-YUEN LOH AND MENG-SING LIOU

Internal Fluid Mechanics Division, NASA Lewis Research Center, Cleveland, Ohio 44135

Received June 2, 1992; revised August 17, 1993

In this paper, the new Lagrangian method introduced by Loh and Hui is extended for 3D steady supersonic flow computation. We present the derivation of the conservation form and the solution of the local Riemann solver using the Godunov and the high resolution TVD schemes. The new approach is accurate and robust, capable of handling complicated geometry and interactions between discontinuous waves. As shown in the test problems, the current Lagrangian method retains all the advantages claimed in the 2D method, e.g., crisp resolution of a slip-surface (contact discontinuity) and automatic grid generation. In this paper, we also suggest a novel 3D Riemann problem in which interesting and intricate flow features are present.

1. INTRODUCTION

It is well known that there exist two formulations describing fluid motion, namely, Eulerian and Lagrangian. The inviscid compressible flow as modelled by the Euler equations of gas dynamics is of both theoretical and practical importance. Over the past four decades much progress has been made in its numerical simulation. Particularly in the 1980s we witnessed an exhaustive exploration of upwind, monotone schemes, notably exact and approximate Riemann solvers, see an extensive review by Roe [1]. However, most of the existing works are based on the Eulerian description of fluid motion, with the exception of one-dimensional flow. On the other hand, back in the fifties and sixties, studies of fluid motion based on the (conventional) Lagrangian description were carried out, most notably in Los Alamos and Lawrence Livermore National Laboratores. One feature of the Lagrangian approach is that the computational grid is embedded in the fluid and distorted with its motion. A major limitation of this approach is its inability to cope with large distortion of the grid when it becomes tangled and highly irregular. Thus, a hybrid Lagrangian–Eulerian approach is attempted (such as the ALE—arbitrary Lagrangian Eulerian method [2]) to recover the grid regularity. Unfortunately, the continuous geometrical interpolation in this hybrid approach eventually leads to loss of accuracy. As a result, since the late sixties, the Eulerian approach wins the upperhand for its easy control of grid and grid regularity. However, the very essence of the Lagrangian approach, that a computational cell being a fluid particle and remaining intact, is missed in the Eulerian one. In the numerical simulation based on the Eulerian description, a slip surface (contact discontinuity), being linearly degenerated, is increasingly smeared as the solution marches further, either in time or in space. In fact, the resolution of contact discontinuity in Eulerian formulation is still a current research topic (e.g., see Harten [3]).

Recently, based on the concept of the *Lagrangian time* introduced by Hui and Van Roessel [5], Loh and Hui [4] derived a new Lagrangian conservation form for the 2D inviscid compressible flow governed by Euler equations and successfully demonstrated its capability in supersonic flow computation. In the new formulation, the *Lagrangian time* τ and the *stream function* ξ replace x and y as the independent variables and the remapping stage is eliminated. They introduced the "geometrical conservation" to overcome the loss of accuracy in geometrical quantities. In the new Lagrangian formulation, a computational cell is literally a fluid particle and flow physics is closely followed. As a result, slipline (contact discontinuity) is crisply resolved, without any detection or artificial treatment, and never smeared further.

In the present paper, we shall extend the new Lagrangian approach of [4] to a three-dimensional steady supersonic flow computation. The extension is not a trivial one since the geometry is complicated and the exact Riemann solution in multi-dimensions is not yet known. Thus we give an approximate approach to the Riemann problem of the present Lagrangian formulation. In Section 2, starting from the three-dimensional Eulerian conservation form, together with the compatibility equations (the *geometrical conservation laws*), we introduce the new Lagrangian conservation form for three-dimensional steady flow. In Section 3, we

0021-9991/94 $6.00

describe the implementation of the Godunov and TVD scheme. In Section 4, we illustrate the so-called pseudo three-dimensional Riemann problem and its solution, which is the basic building block in Section 3. In Section 5, we briefly discuss the well-posedness of the Cauchy problem in question. The well-posedness or the general CFL condition controls the stability of the numerical procedure. It is shown how this condition is easily met in the present Lagrangian approach. Through several test examples in Section 6, we shall show the robustness and accuracy of the new approach. Finally, the paper is completed with our concluding remarks.

2. THE NEW LAGRANGIAN CONSERVATION FORM FOR THREE-DIMENSIONAL STEADY FLOWS

For any modern shock-capturing scheme, an appropriate conservation form is essential for the accuracy. We begin the derivation of the Lagrangian conservation form with the Eulerian conservation laws written for three-dimensional steady flows,

$$\frac{\partial \mathbf{E}}{\partial x}+\frac{\partial \mathbf{F}}{\partial y}+\frac{\partial \mathbf{G}}{\partial z}=0, \tag{1}$$

where

$$\mathbf{E}=\begin{pmatrix} \rho u \\ \rho u^2+p \\ \rho uv \\ \rho uw \\ \rho uH \end{pmatrix}, \quad \mathbf{F}=\begin{pmatrix} \rho v \\ \rho vu \\ \rho v^2+p \\ \rho vw \\ \rho vH \end{pmatrix}, \quad \mathbf{G}=\begin{pmatrix} \rho w \\ \rho wu \\ \rho wv \\ \rho w^2+p \\ \rho wH \end{pmatrix}.$$

As usual, u, v, w, ρ, and p are respectively the Cartesian components of flow velocity, density, and pressure of the fluid obeying the γ-law; the total enthalpy

$$H=\frac{1}{2}(u^2+v^2+w^2)+\frac{\gamma}{(\gamma-1)}\frac{p}{\rho}, \qquad \gamma=1.4.$$

Recently, Loh and Hui [4] introduce a new Lagrangian conservation form for two-dimensional steady supersonic flow computation, which is based on the concept of Lagrangian time [5, 6]. The Lagrangian time is indeed a physical time—the time of motion of each fluid particle along its own streamline. For each fluid particle, following its streamline the Lagrangian time differs from the physical time t only by a constant t_0:

$$\tau=t+t_0 \tag{2}$$

which may be regarded as the local initial time associated with each fluid particle. In this formulation τ and the stream function ξ replace x and y as the independent variables. A computational cell is literally a fluid particle and the flow physics is closely followed. The Lagrangian approach possesses many attractive features that are missed in the Eulerian one, such as crisp resolution of slipline and automatic grid generation.

In an attempt to explore a Lagrangian approach for higher dimensions, in this section we shall extend the new Lagrangian formulation in [4] to a three-dimensional one and derive the corresponding conservation form. There are two types of Lagrangian conservation form [7]. The basic one is based on Lagrangian time τ and the enhanced one based on the "Lagrangian distance" λ. By Lagrangian distance we mean the distance (arc length) along a streamline. In the presence of strong contact discontinuities or slip-surfaces the latter does a better job in numerical computations. In this paper, we shall use for our computation the conservation form based on the "Lagrangian distance" λ (the λ conservation form). It is noted that this form can be derived from the τ-formulation as we have chosen to do in the present paper, or directly from the original Euler equations.

It is well known that in a three-dimensional steady flow, there exist two independent stream functions, say, ξ and η. Each fixed ξ or η represents a stream surface (Fig. 1a). A fixed pair of ξ and η denotes a streamline in the three-dimensional space. Following the streamline, the Lagrangian time τ or the Lagrangian distance λ uniquely determines the location of the fluid particle. In other words, for example, (τ, ξ, η) may be considered as a new set of independent variables, which are now functions of the Cartesian coordinates $\mathbf{r}=(x, y, z)^{\mathrm{T}}$. Since (2) holds along a streamline (on which ξ, η are held fixed), the fluid velocity $\mathbf{V}$ is

$$\mathbf{V}=(u, v, w)^{\mathrm{T}}=\frac{\partial \mathbf{r}}{\partial t}=\frac{\partial \mathbf{r}}{\partial \tau}. \tag{3}$$

Furthermore, we define the Lagrangian quantities

$$\mathbf{T}=(U, V, W)^{\mathrm{T}}=\frac{\partial \mathbf{r}}{\partial \xi}, \qquad \mathbf{S}=(X, Y, Z)^{\mathrm{T}}=\frac{\partial \mathbf{r}}{\partial \eta}; \tag{4}$$

these quantities represent the lateral rate of displacement of a fluid particle (or computational cell). The determinant of the Jacobian J,

$$|J|=\left|\frac{\partial(x, y, z)}{\partial(\tau, \xi, \eta}\right|=\begin{vmatrix} u & v & w \\ U & V & W \\ X & Y & Z \end{vmatrix}, \tag{5}$$

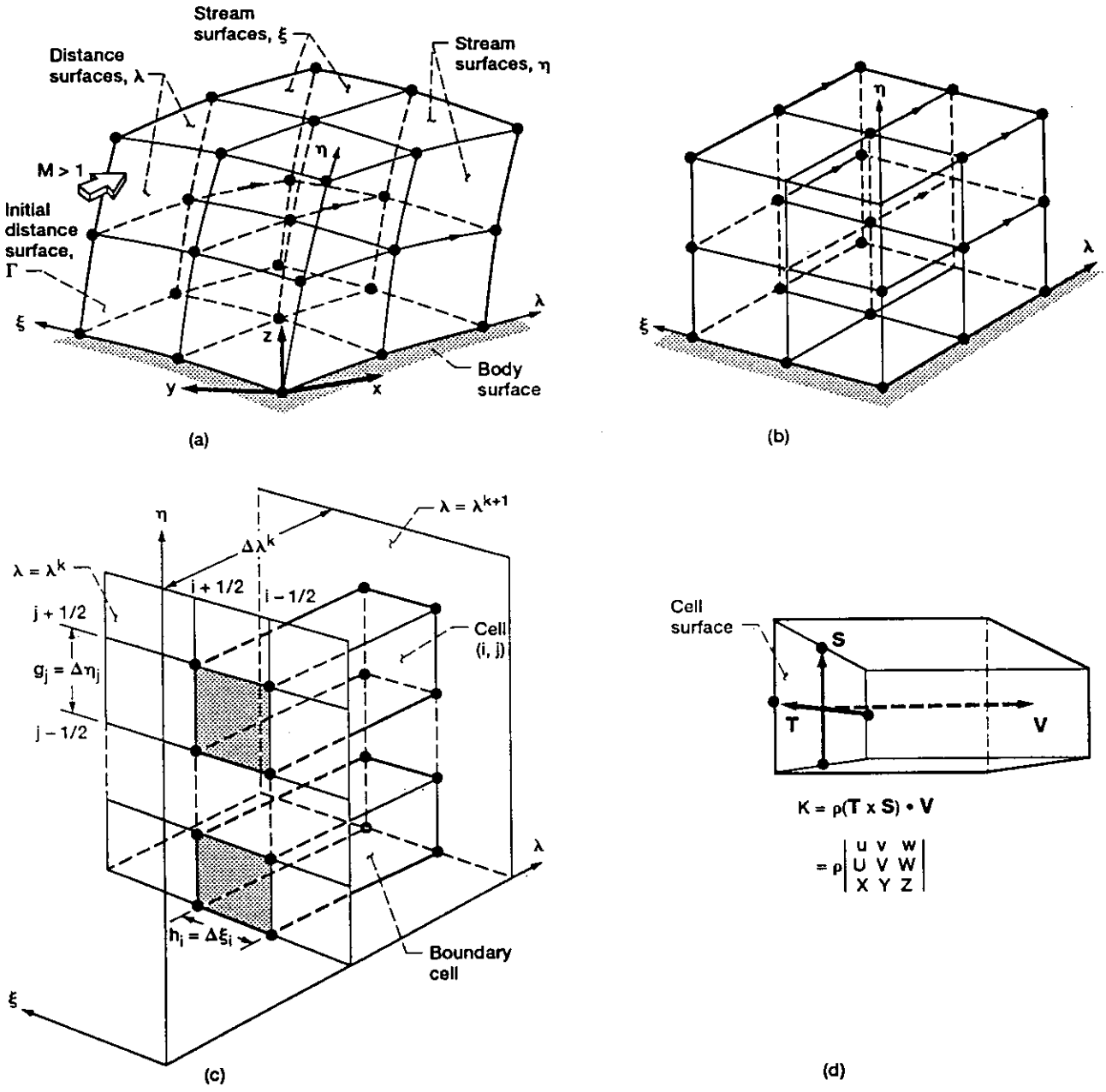

FIG. 1. Computational space and mesh.

denotes the volume ratio during the change of independent variables. Subsequently, similar to [4],

$$K = \rho\,|J| = \rho \begin{vmatrix} u & v & w \\ U & V & W \\ X & Y & Z \end{vmatrix}, \tag{6}$$

is the mass flux (Fig. 1d).

We also note that the following relations are the compatibility conditions between the τ-derivatives, ξ-derivatives, and η-derivatives of x, y, and z,

$$\frac{\partial \mathbf{T}}{\partial \tau} = \frac{\partial \mathbf{V}}{\partial \xi}, \qquad \frac{\partial \mathbf{S}}{\partial \tau} = \frac{\partial \mathbf{V}}{\partial \eta}, \qquad \frac{\partial \mathbf{T}}{\partial \eta} = \frac{\partial \mathbf{S}}{\partial \xi}. \tag{7}$$

Starting with the Eulerian conservation form (1) and the relations (3)–(7), we can perform the variable transformation from (x, y, z) to (τ, ξ, η) and achieve the conservation

form based on Lagrangian time τ. In this τ conservation form, each fluid particle marches forward with the same time step $\Delta\tau$ according to its own velocity. Across a contact discontinuity (slip surface) where flow velocity may be discontinuous, two adjacent fluid particles initially in physical contact may eventually be separated from each other, rendering it difficult to apply a local Riemann solver in the Godunov/TVD schemes. A remedy is to keep these two particles marching in the same pace. More generally, we can let all the fluid particles march the same distance $\Delta\lambda$ instead of the same time step $\Delta\tau$ along their own streamlines. This idea leads to another new Lagrangian conservation form—the conservation form based on the Lagrangian distance λ. Hui and Zhao have all the details in their recent paper [7]. We present here only a sketch of the necessary steps.

First, we define the Lagrangian distance as

$$\lambda = \int_0^\tau q \, d\tau, \tag{8a}$$

where the flow speed

$$q = (u^2 + v^2 + w^2)^{1/2}.$$

The other independent variables are the same as before:

$$\begin{aligned} \xi_1 &= \xi \\ \eta_1 &= \eta. \end{aligned} \tag{8b}$$

Let

$$\alpha = \frac{\partial \lambda}{\partial \xi}, \qquad \beta = \frac{\partial \lambda}{\partial \eta}.$$

From (8), two useful relations can be easily derived:

$$\frac{\partial \alpha}{\partial \lambda} = \frac{1}{q}\frac{\partial q}{\partial \xi}, \qquad \frac{\partial \beta}{\partial \lambda} = \frac{1}{q}\frac{\partial q}{\partial \eta}. \tag{9}$$

Now, we can make the coordinate transformation from (λ, ξ_1, η_1) to (τ, ξ, η) and the Jacobian J_1 is

$$J_1 = \frac{\partial(\lambda, \xi_1, \eta_1)}{\partial(\tau, \xi, \eta)} = \begin{pmatrix} \partial\lambda/\partial\tau & \partial\xi_1/\partial\tau & \partial\eta_1/\partial\tau \\ \partial\lambda/\partial\xi & \partial\xi_1/\partial\xi & \partial\eta_1/\partial\xi \\ \partial\lambda/\partial\eta & \partial\xi_1/\partial\eta & \partial\eta_1/\partial\eta \end{pmatrix} = \begin{pmatrix} q & 0 & 0 \\ \alpha & 1 & 0 \\ \beta & 0 & 1 \end{pmatrix}.$$

The inversed J_1 is

$$J_1^{-1} = \frac{\partial(\tau, \xi, \eta)}{\partial(\lambda, \xi_1, \eta_1)} = \begin{pmatrix} \partial\tau/\partial\lambda & \partial\xi/\partial\lambda & \partial\eta/\partial\lambda \\ \partial\tau/\partial\xi_1 & \partial\xi/\partial\xi_1 & \partial\eta/\partial\xi_1 \\ \partial\tau/\partial\eta_1 & \partial\xi/\partial\eta_1 & \partial\eta/\partial\eta_1 \end{pmatrix} = \begin{pmatrix} 1/q & 0 & 0 \\ -\alpha/q & 1 & 0 \\ -\beta/q & 0 & 1 \end{pmatrix}.$$

Our final goal is a transformation from (x, y, z) to (λ, ξ_1, η_1), which can be achieved via successive coordinate transformations: $(x, y, z) \Leftrightarrow (\tau, \xi, \eta) \Leftrightarrow (\lambda, \xi_1, \eta_1)$. The resultant Jacobian J_0 is

$$\begin{aligned} J_0 &= \frac{\partial(x, y, z)}{\partial(\lambda, \xi_1, \eta_1)} = \frac{\partial(\tau, \xi, \eta)}{\partial(\lambda, \xi_1, \eta_1)} \frac{\partial(x, y, z)}{\partial(\tau, \xi, \eta)} \\ &= \begin{pmatrix} 1/q & 0 & 0 \\ -\alpha/q & 1 & 0 \\ -\beta/q & 0 & 1 \end{pmatrix} \begin{pmatrix} u & v & w \\ U & V & W \\ X & Y & Z \end{pmatrix} \\ &= \begin{pmatrix} u/q & v/q & w/q \\ U - \alpha u/q & V - \alpha v/q & W - \alpha w/q \\ X - \beta u/q & Y - \beta v/q & Z - \beta w/q \end{pmatrix}. \end{aligned}$$

By inverting the Jacobian J_0 we have

$$J_1^{-1} = \frac{\partial(\lambda, \xi_1, \eta_1)}{\partial(x, y, z)} = \begin{pmatrix} \partial\lambda/\partial x & \partial\xi_1/\partial x & \partial\eta_1/\partial x \\ \partial\lambda/\partial y & \partial\xi_1/\partial y & \partial\eta_1/\partial y \\ \partial\lambda/\partial z & \partial\xi_1/\partial z & \partial\eta_1/\partial z \end{pmatrix} = \frac{q\rho}{K} \begin{pmatrix} J_{11} & J_{21} & J_{31} \\ J_{12} & J_{22} & J_{32} \\ J_{13} & J_{23} & J_{33} \end{pmatrix}. \tag{10}$$

Here, J_{rs} $(r, s = 1, 2, 3)$ are the cofactors of the determinant $|J_0|$. We also note that the determinant

$$|J_0| = \frac{|J|}{q} = \frac{K}{\rho q}.$$

Equation (10) provides all the partial derivatives $\partial/\partial x$, $\partial/\partial y$, and $\partial/\partial z$ that are needed in converting the Eulerian conservation form (1) into a new Lagrangian conservation form with (λ, ξ_1, η_1) as the independent variables:

$$\begin{aligned} \frac{\partial}{\partial x} &= \frac{\rho q}{K}\left(J_{11}\frac{\partial}{\partial \lambda} + J_{21}\frac{\partial}{\partial \xi_1} + J_{31}\frac{\partial}{\partial \eta_1}\right), \\ \frac{\partial}{\partial y} &= \frac{\rho q}{K}\left(J_{12}\frac{\partial}{\partial \lambda} + J_{22}\frac{\partial}{\partial \xi_1} + J_{32}\frac{\partial}{\partial \eta_1}\right), \\ \frac{\partial}{\partial z} &= \frac{\rho q}{K}\left(J_{31}\frac{\partial}{\partial \lambda} + J_{23}\frac{\partial}{\partial \xi_1} + J_{33}\frac{\partial}{\partial \eta_1}\right). \end{aligned}$$

After some algebraic manipulation, (1) is transformed into a new Lagrangian λ conservation form:

$$\frac{\partial}{\partial\lambda}\begin{pmatrix} K \\ Ku+pJ_{11} \\ Kv+pJ_{12} \\ Kw+pJ_{13} \\ HK \end{pmatrix}+\frac{\partial}{\partial_1}\begin{pmatrix} 0 \\ pJ_{21} \\ pJ_{22} \\ pJ_{23} \\ 0 \end{pmatrix}+\frac{\partial}{\partial\eta_1}\begin{pmatrix} 0 \\ pJ_{31} \\ pJ_{32} \\ pJ_{33} \\ 0 \end{pmatrix}=0. \tag{11}$$

We note that the first equation in (11) implies that $K=$ constant along a streamline and hence the fifth equation is reduced to

$$\frac{\partial H}{\partial\lambda}=0.$$

Moreover, corresponding to (4), we define $\mathbf{T}_1$ and $\mathbf{S}_1$ as the line vectors of the Jacobian J_0, i.e.,

$$\mathbf{T}_1=\mathbf{T}-\alpha\mathbf{V}/q, \qquad \mathbf{T}_1=(U_1, V_1, W_1)^{\mathrm{T}},$$
$$\mathbf{S}_1=\mathbf{S}-\beta\mathbf{V}/q, \qquad \mathbf{S}_1=(X_1, Y_1, Z_1)^{\mathrm{T}}.$$

These vectors represent the geometrical deformation of the computational cells (fluid particles). Similar to the compability equations (7), it can be shown, by using (7) and (9) that

$$\frac{\partial\mathbf{T}_1}{\partial\lambda}=\frac{\partial\mathbf{V}/q}{\partial\xi_1},$$
$$\frac{\partial\mathbf{S}_1}{\partial\lambda}=\frac{\partial\mathbf{V}/q}{\partial\eta_1}, \tag{12}$$
$$\frac{\partial\mathbf{T}_1}{\partial\eta_1}=\frac{\partial\mathbf{S}_1}{\partial\xi_1}.$$

Combining (11) and (12) and then dropping the subscript "1," we achieve a complete set of the new Lagrangian conservation form based on the λ-variable,

$$\frac{\partial\mathbf{E}}{\partial\lambda}+\frac{\partial\mathbf{F}}{\partial\xi}+\frac{\partial\mathbf{G}}{\partial\eta}=0, \tag{13}$$

where

$$\mathbf{E}=\begin{pmatrix} e_1 \\ e_2 \\ e_3 \\ e_4 \\ e_5 \\ e_6 \\ e_7 \\ e_8 \\ e_9 \\ e_{10} \\ e_{11} \end{pmatrix}\equiv\begin{pmatrix} K \\ H \\ Ku+pJ_{11} \\ Kv+pJ_{12} \\ Kw+pJ_{13} \\ U \\ V \\ W \\ X \\ Y \\ Z \end{pmatrix},$$

$$\mathbf{F}=\begin{pmatrix} 0 \\ 0 \\ pJ_{21} \\ pJ_{22} \\ pJ_{23} \\ -u/q \\ -v/q \\ -w/q \\ 0 \\ 0 \\ 0 \end{pmatrix}, \qquad \mathbf{G}=\begin{pmatrix} 0 \\ 0 \\ pJ_{31} \\ pJ_{32} \\ pJ_{33} \\ 0 \\ 0 \\ 0 \\ -u/q \\ -v/q \\ -w/q \end{pmatrix}.$$

In (13), the third equation in (12) is ignored since it has no contribution to $\mathbf{E}$ and is automatically satisfied.

As noted earlier, the Lagrangian conservation form (13) can, of course, be directly derived from the very first principles of physics and the compatibility equations by considering the computational cell as a segment of the stream tube between two marching surfaces.

The system (13) may look overwhelming at first glance and could be rejected prematurely. However, further examination reveals many simplifications and identities. The first two equations simply imply that $H=$ const, $K=$ const along a streamline. For steady supersonic flows, one needs only to handle the rest of the nine equations in order to march forward and solve the system. Among them, the six compatibility equations for $e_6, e_7, \ldots, e_{11}$ can be solved in a straightforward way, as will be seen in next section, and only the three momentum equations for e_3, e_4, and e_5 require more attention in the numerical procedure.

3. APPLICATION OF GODUNOV AND TVD SCHEMES

For a supersonic flow with the overall Mach number $M>1$ everywhere, the system (13) is of hyperbolic type. Details about the hyperbolicity of (13) are included in the Appendix at the end of the paper. In the past four decades various numerical methods have been developed to handle the hyperbolic systems; there exists a complete spectrum of shock-capturing finite difference/finite volume schemes to solve the hyperbolic system of conservation laws, such as Godunov, flux-splitting, TVD, UNO, ENO, etc. In the present paper, as an early exploration of the new 3D Lagrangian method, we apply the basic Godunov scheme and then upgrade it to a high resolution TVD scheme.

3.1. *Application of Godunov Scheme*

The physical domain and computational domain in the λ-ξ-η space are respectively illustrated in Figs. 1a and 1b. A cuboid mesh in the computational domain is used and the computation marches in Lagrangian distance λ. The super-

script k refers to the marching step number and the subscripts i and j refer to the cell number on the distance plane (λ plane with $\lambda = \text{const}$). The marching step $\Delta\lambda^k = \lambda^{k+1} - \lambda^k$ is uniform for all i and j. It may vary with k, but it is always chosen to satisfy the usual CFL linear stability condition. The mesh divides the computational domain into cuboid control volumes or cells which in the ξ and η direction are centered at $(\lambda^k, \xi_i, \eta_j)$ and have heights $\Delta\xi_i = \xi_{i+1/2} - \xi_{i-1/2}$ and $\Delta\eta_j = \eta_{j+1/2} - \eta_{j-1/2}$ (for all k). Unless otherwise stated we shall use uniform cell width $\Delta\xi_i$ for all i and $\Delta\eta_j$ for all j.

In the physical space a cuboid cell marching in (λ, ξ, η) space corresponds to a fluid particle marching along its stream tube with step $\Delta\lambda$. The fluid particle is bounded by four stream surface $\xi = \xi_{i\pm 1/2}$ and $\eta = \eta_{j\pm 1/2}$ around it (Fig. 1c). The $\xi - \eta$ plane in computational space corresponds to the initial surface in the physical space. Any curvilinear coordinate mesh on the initial surface may be used as the ξ-η coordinate mesh and the initial $\mathbf{T}$ and $\mathbf{S}$ can be determined as part of the initial condition. A solid wall is always a stream surface and, hence, a coordinate surface.

The finite difference scheme of Godunov [9] for (13) is derived by applying the divergence theorem to the cuboid cell (i, j, k). The result is

$$\mathbf{E}_{i,j}^{k+1} = \mathbf{E}_{i,j}^{k} - \frac{\Delta\lambda^k}{\Delta\xi_i}(\mathbf{F}_{i+1/2,j}^{k+1/2} - \mathbf{F}_{i-1/2,j}^{k+1/2}) - \frac{\Delta\lambda^k}{\Delta\eta_j}(\mathbf{G}_{i,j+1/2}^{k+1/2} - \mathbf{G}_{i,j-1/2}^{k+1/2}),$$
$$i = 1, 2, \ldots, m; \quad j = 1, 2, \ldots, n, \tag{14}$$

where the notation for the cell average of any quantity f is

$$f_{i,j}^{k} = \frac{1}{\Delta\xi_i\,\Delta\eta_j}\int_{\xi_{i-1/2}}^{\xi_{i+1/2}}\int_{\eta_{j-1/2}}^{\eta_{j+1/2}} f(\lambda^k, \xi, \eta)\,d\xi\,d\eta, \tag{15}$$

and the notation for λ average of f is

$$f_{i+1/2,j}^{k+1/2} = \frac{1}{\Delta\lambda^k}\int_{\lambda^k}^{\lambda^{k+1}} f(\lambda, \xi_{i+1/2}, \eta_j)\,d\lambda, \tag{16}$$

$$f_{i,j+1/2}^{k+1/2} = \frac{1}{\Delta\lambda^k}\int_{\lambda^k}^{\lambda^{k+1}} f(\lambda, \xi_i, \eta_{j+1/2})\,d\lambda. \tag{17}$$

In (14) the cell-interface fluxes $\mathbf{F}_{i+1/2,j}^{k+1/2}$ and $\mathbf{G}_{i,j+1/2}^{k+1/2}$ for the cell (i, j) are to be obtained from the self-similar solution of a local three-dimensional Riemann problem formed by the average constant state $\mathbf{Q}_{i,j} = (u, v, w, p, \rho)_{i,j}^{\mathrm{T}}$ of the cell (i, j) and those of its adjacent cells (Fig. 2a). Unfortunately, due to its complexity, the exact solution to a general three-dimensional Riemann problem is not yet available [10]. On the other hand, it is known that a montone difference scheme to a general conservation form converges to the physically relevant entropy-satisfying solution (see Harten *et al.* [11]). In particular, Crandall and Majda [12] establish the rigorous convergence for dimensional splitting algorithms when each step is approximated by a monotone difference scheme (such as the Godunov scheme) for a single conservation law of multi-dimensions. We shall extend and apply the dimensional splitting in the Godunov scheme for our hyperbolic system of conservation laws (13).

When applying the dimension-splitting technique in the Godunov scheme for (13), one only needs to solve a pseudo three-dimensional Riemann problem formed by two adjacent constant states, say, $\mathbf{Q}_{i,j}$ and $\mathbf{Q}_{i+1,j}$ instead of genuine three-dimensional ones (Figs. 2a and 2b). In fact, a pseudo three-dimensional Riemann problem is identical to a two-dimensional one [4], except that the direction of the interaction line of the two constant states must be known. We have more details about the pseudo three-dimensional Riemann problem in the next section.

The interaction between two 3D supersonic flows of constant states separated by a plane is much more complicated than in the 2D case. The interaction line is designed to handle this situation. It is the line at which the two three-dimensional flows begin to contact and interact with each other (Fig. 2b and Fig. 3). In order to find the direction or the unit vector of the interaction line and solve the corresponding pseudo-three-dimensional Riemann problem, in which we are given cells (i, j) and $(i+1, j)$, $(\mathbf{Q}_{i,j}, \mathbf{T}_{i,j}, \mathbf{S}_{i,j})$, and $(\mathbf{Q}_{i+1,j}, \mathbf{T}_{i+1,j}, \mathbf{S}_{i+1,j})$, we recommend two approaches.

In the first approach, we consider the interaction line as the intersection line of two adjacent λ surfaces and the following two steps are followed (Fig. 2c):

(a) Calculate the unit normal vectors of the λ surface of Cells (i, j) and $(i+1, j)$:

$$\mathbf{n}_{i,j} = \frac{\mathbf{T}_{i,j}\times\mathbf{S}_{i,j}}{|\mathbf{T}_{i,j}\times\mathbf{S}_{i,j}|}, \qquad \mathbf{n}_{i+1,j} = \frac{\mathbf{T}_{i+1,j}\times\mathbf{S}_{i+1,j}}{|\mathbf{T}_{i+1,j}\times\mathbf{S}_{i+1,j}|}.$$

If the cell is a boundary cell, i.e., one or more of its walls is a given solid body surface, and interacting with the solid boundary (Fig. 2d), we still calculate the unit normal corresponding to the cell (i, j):

$$\mathbf{n}_{i,j} = \frac{\mathbf{T}_{i,j}\times\mathbf{S}_{i,j}}{|\mathbf{T}_{i,j}\times\mathbf{S}_{i,j}|}.$$

(b) Calculate $\mathbf{m}_1 = \mathbf{n}_{i,j}\times\mathbf{n}_{i+1,j}$, the directional vector of the interaction line. If $|\mathbf{m}_1| < \varepsilon$, where ε is a threshold value to avoid possible ill-conditionedness and filter possible noise, then discard the present, $\mathbf{m}_1$ and use the one of the previous time step. We find $\varepsilon = 0.05$ is quite appropriate in all our numerical examples. Then $\mathbf{m}_1$ is normalized to a unit vector. If a solid wall is present,

$$\mathbf{m}_1 = \mathbf{n}_{\text{wall}}\times\mathbf{n}_{i,j}.$$

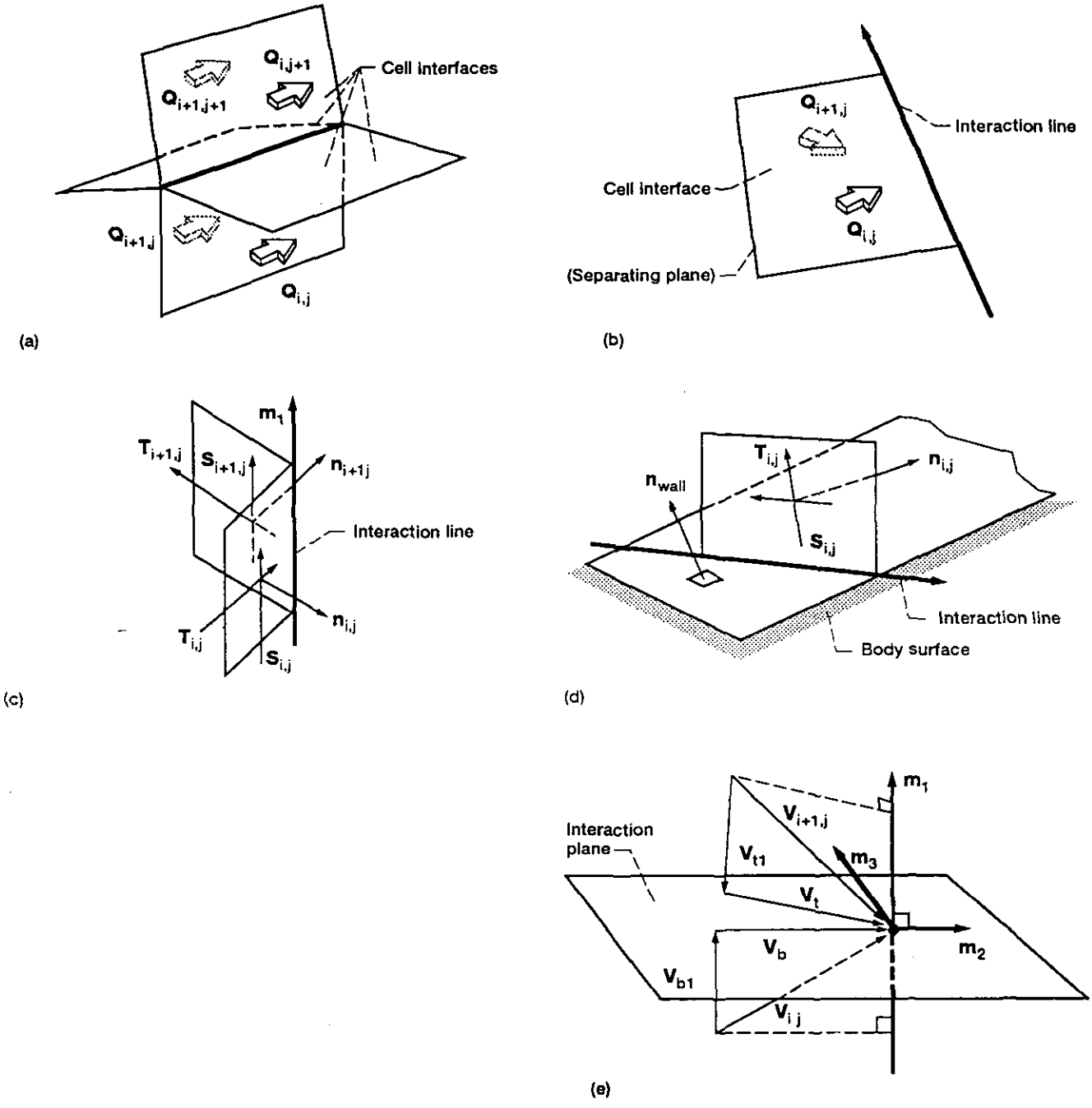

FIG. 2. Determination of the interaction line: (a) typical 3D Riemann problem in the Godunov scheme; (b) pseudo 3D Riemann problem with initial states $\mathbf{Q}_{ij}\mathbf{Q}_{i+1,j}$; (c) interaction line direction for a pseudo 3D Riemann problem; (d) interaction line direction for a pseudo 3D boundary Riemann problem; (e) initial data for a standard 2D Riemann problem on the interacting plane.

Here we assume the unit normal vector $\mathbf{n}_{\text{wall}}$ of the solid body surface is given as a boundary condition. On the initial surface, $\mathbf{m}_1$ is specified as the unit vector of cell interface lines.

The second approach is to reconstruct the cell edge (i.e., the interaction line) by averaging cell center locations. For example, the cell edge between cells (i,j) and $(i+1,j)$ can be obtained by connecting the two vertices, one being the average of the center locations of cells $(i+1,j)$, (i,j), $(i+1,j+1)$, $(i,j+1)$ and the other the average of center locations of cells (i,j), $(i-1,j)$, $(i,j+1)$, $(i-1,j+1)$ (Fig. 2e). Therefore, the directional vector (to be normalized) $\mathbf{m}_1$ has a simple form

$$\mathbf{m}_1 = (m_{1x}, m_{1y}, m_{1z})^{\mathrm{T}}$$

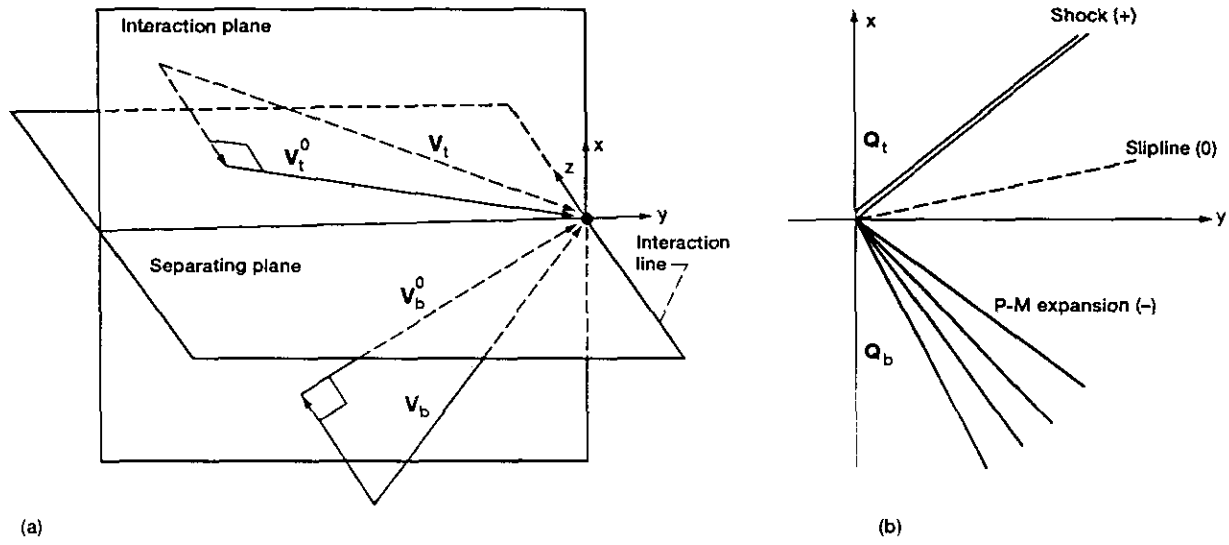

FIG. 3. The pseudo 3D Riemann problem: (a) reduction of a pseudo 3D Riemann problem to a 2D Riemann problem; (b) the 2D Riemann problem.

with the components

$$m_{1x} = x_{i+1,j+1} + x_{i+1,j} - x_{i-1,j+1} - x_{i-1,j}$$
$$m_{1y} = y_{i+1,j+1} + y_{i+1,j} - y_{i-1,j+1} - y_{i-1,j}$$
$$m_{1z} = z_{i+1,j+1} + z_{i+1,j} - z_{i-1,j+1} - z_{i-1,j}.$$

Comparing to the above interaction line approach steps (a) and (b), this one is much simpler and seemingly more consistent. In our numerical experiments with these two approaches, the results are practically identical.

Once the interaction line is known, from which we construct a local Cartesian coordinate system and apply a usual 2D Riemann solver in the following way. The validity of doing so will be described in the next section.

(c) Project the flow velocity vector $\mathbf{V}_{i,j}$ on the plane perpendicular to $\mathbf{m}_1$ (the interaction plane, Fig. 2f, Fig. 3) to obtain $\mathbf{V}_b$, V_b is then normalized to give $\mathbf{m}_2$—the second unit vector, which is normal to $\mathbf{m}_1$ as well. In the mean time, $\mathbf{V}_{i+1,j}$ is projected on the same interaction plane, yielding $\mathbf{V}_t$,

$$\mathbf{V}_{i,j} = \mathbf{V}_b + \mathbf{V}_{b1},$$
$$\mathbf{V}_{i+1,j} = \mathbf{V}_t + \mathbf{V}_{t1},$$

together with

$$\mathbf{V}_{b1} = (\mathbf{V}_{i,j} \cdot \mathbf{m}_1)\,\mathbf{m}_1,$$
$$\mathbf{V}_{t1} = (\mathbf{V}_{i+1,j} \cdot \mathbf{m}_1)\,\mathbf{m}_1,$$

where the subscripts "b" and "t" correspond to bottom and top states (see the next section) which are the counterparts of right and left states in one-dimensional unsteady flow.

(d) Let $\mathbf{m}_3 = \mathbf{m}_1 \times \mathbf{m}_2$, then, $\mathbf{m}_1$, $\mathbf{m}_2$, $\mathbf{m}_3$ form a local right-hand Cartesian coordinate system. $\mathbf{m}_2$ and $\mathbf{m}_3$ span the interaction plane, in which we have two constant states:

$$\mathbf{Q}_b = (u_b, v_b, p_b, \rho_b)^{\mathrm{T}} = (|\mathbf{V}_b|, 0, p_{i,j}, \rho_{i,j}),$$
$$\mathbf{Q}_t = (u_t, v_t, p_t, \rho_t)^{\mathrm{T}} = (\mathbf{V}_t \cdot \mathbf{m}_2, \mathbf{V}_t \cdot \mathbf{m}_3, p_{i+1,j}, \rho_{i+1,j}).$$

Then a standard 2D Riemann solver (see the next section) can be used to solve for new $\mathbf{Q}_b$ and $\mathbf{Q}_t$. If the cell is a boundary cell interacting with the solid boundary, the data of $\mathbf{Q} = \mathbf{Q}_t$ is enough for computing new $\mathbf{Q}$ via a standard two-dimensional boundary Riemann solver.

(e) Recover new interface three-dimensional states for the purpose of computing cell interface fluxes:

$$\mathbf{V}^{k+1/2}_{i+1/2,j} = u_b \mathbf{m}_2 + v_b \mathbf{m}_3 + \mathbf{V}_{b1}, \qquad p^{k+1/2}_{i+1/2,j} = p_b.$$

The same procedure (a)–(e) is to carry out for all four cell interfaces around the cell (i,j), namely, the interfaces $(i \pm 1/2, j \pm 1/2)$ (Fig. 1c).

In the first-order Godunov scheme the cell average $\mathbf{E}^k_{i,j}$ at time step k is considered as constant within the cell (i,j) and the fluxes $\mathbf{F}^{k+1/2}_{i+1/2,j}$ along the interface between cells (i,j) and $(i+1,j)$ and $\mathbf{G}^{k+1/2}_{i,j+1/2}$ along the interface between cells (i,j) and $(i,j+1)$ from step k to step $k+1$ are obtained as in (16) and (17). Due to the self-similarity of the solution of the pseudo-three-dimensional Riemann problem, for any components f of fluxes $\mathbf{F}$ and $\mathbf{G}$, (16) and (17) may be reduced to

$$f^{k+1/2}_{i+1/2,j} = f(\lambda^{k+1/2}, \xi_{i+1/2}, \eta_j), \tag{18}$$
$$f^{k+1/2}_{i,j+1/2} = f(\lambda^{k+1/2}, \xi_i, \eta_{j+1/2}). \tag{19}$$

from (13), we see that f is a simple function of $\mathbf{Q}$, $\mathbf{T}$, and $\mathbf{S}$.

Now we summarize the complete numerical procedure of Godunov method:

(i) *Initiation.* Given a three-dimensional flow problem in the Cartesian (x, y, z)-space, we choose a surface Γ, not itself a stream surface, on which the flow is known (e.g., a given uniform flow), as the initial surface $\lambda = 0$ (Fig. 1a). Then a parameterized curvilinear $\xi - \eta$ coordinate mesh is laid on Γ (for instance, we take ξ and η equal to the arc length of their corresponding coordinate lines on Γ), with

$$\xi = \xi_0, \xi_1, \xi_2, ..., \xi_m; \qquad \eta = \eta_0, \eta_1, \eta_2, ..., \eta_n,$$

and ξ_0 and/or η_0 coinciding with the solid body surfaces (Fig. 1). Hence $\mathbf{T}^0$, $\mathbf{S}^0$, as well as the flow variable $\mathbf{Q}^0$, are known on Γ as initial conditions. Then $\mathbf{E}^0_{i,j}$ are known on Γ as well. In most of the test examples of the present paper, we take the uniform free stream as the x-direction, $y-z$ plane as the initial surface Γ, and choose ξ, η to be the respective arc lengths of y- and z-coordinate lines. This results in $\mathbf{T}^0 = (0, 1, 0)^{\mathrm{T}}$, $\mathbf{S}^0 = (0, 0, 1)^{\mathrm{T}}$, and the averaged $\mathbf{E}^0$ follows from (15) in a straightforward way.

(ii) With all $\mathbf{E}^k_{i,j}$ and $\mathbf{Q}^k_{i,j}$ known at step k $(k = 0, 1, 2, ...)$, solve the local pseudo-three-dimensional Riemann problems (or local boundary Riemann problem) at the cell interfaces and obtain the cell interface flow variables: $\mathbf{V}^{k+1/2}_{i\pm 1/2,j}$ or $\mathbf{V}^{k+1/2}_{i\pm 1/2,j}$ and $p^{k+1/2}_{i\pm 1/2,j}$ or $p^{k+1/2}_{i\pm 1/2,j}$ as described in the above context. Then fluxes $\mathbf{F}$ and $\mathbf{G}$ are calculated from (18) and (19), or more explicitly, from the $\mathbf{F}$ and $\mathbf{G}$ expressions in (13). In order to do so, we first update $\mathbf{T}^k_{i,j}$ and $\mathbf{S}^k_{i,j}$ to $\mathbf{T}^{k+1}_{i,j}$ and $\mathbf{S}^{k+1}_{i,j}$:

$$\begin{pmatrix} U^{k+1}_{i,j} \\ V^{k+1}_{i,j} \\ W^{k+1}_{i,j} \end{pmatrix} = \mathbf{T}^{k+1}_{i,j} = \mathbf{T}^k_{i,j} - \frac{\Delta\lambda^k}{\Delta\xi_i} \times \left(\frac{\mathbf{V}^{k+1/2}_{i+1/2,j}}{q^{k+1/2}_{i+1/2,j}} - \frac{\mathbf{V}^{k+1/2}_{i-1/2,j}}{q^{k+1/2}_{i-1/2,j}} \right), \tag{20}$$

$$\begin{pmatrix} X^{k+1}_{i,j} \\ Y^{k+1}_{i,j} \\ Z^{k+1}_{i,j} \end{pmatrix} = \mathbf{S}^{k+1}_{i,j} = \mathbf{S}^k_{i,j} - \frac{\Delta\hat{\lambda}^k}{\Delta\eta_j} \times \left(\frac{\mathbf{V}^{k+1/2}_{i,j+1/2}}{q^{k+1/2}_{i,j+1/2}} - \frac{\mathbf{V}^{k+1/2}_{i,j-1/2}}{q^{k+1/2}_{i,j-1/2}} \right), \tag{21}$$

$$i = 1, 2, ..., m; \quad j = 1, 2, ..., n; \quad k = 0, 1, 2, ...$$

Thus the calculation of the sixth to the eleventh components of the interface fluxes $\mathbf{F}$ and $\mathbf{G}$, and the updating of U, V, W, X, Y, and Z (i.e., $e_6, e_7, ..., e_{11}$) are now complete. With $(U, V, W)^{\mathrm{T}}$ and $(X, Y, Z)^{\mathrm{T}}$ from (20), (21), the computed cell-interface $\mathbf{V}^{k+1/2}_{i\pm 1/2,j}$ or $\mathbf{V}^{k+1/2}_{i,j\pm 1/2}$ from the pseudo 3D Riemann solver, the cofactors J_{rs} $(r = 2, 3, s = 1, 2, 3)$ at the cell interfaces can be calculated according to the following list:

$$J_{21} = -\frac{1}{q}\begin{vmatrix} v & w \\ Y & Z \end{vmatrix}, \quad J_{22} = \frac{1}{q}\begin{vmatrix} u & w \\ X & Z \end{vmatrix}, \quad J_{23} = -\frac{1}{q}\begin{vmatrix} u & v \\ X & Y \end{vmatrix},$$

$$J_{31} = \frac{1}{q}\begin{vmatrix} v & w \\ V & W \end{vmatrix}, \quad J_{32} = -\frac{1}{q}\begin{vmatrix} u & w \\ U & W \end{vmatrix}, \quad J_{33} = \frac{1}{q}\begin{vmatrix} u & v \\ U & V \end{vmatrix}.$$

Furthermore, by utilizing the cell-interface pressure $p^{k+1/2}_{i\pm 1/2,j}$ or $p^{k+1/2}_{i,j\pm 1/2}$ and J_{rs}, the third, fourth, and fifth components of the interface fluxes $\mathbf{F}$ and $\mathbf{G}$ are calculated according to their expressions in (13). For example, for the cell (i, j), the third component of $\mathbf{F}$ at the interface between cells $(i+1, j)$ and (i, j) is evaluated as

$$-\frac{p^{k+1/2}_{i+1/2,j}}{q^{k+1/2}_{i+1/2,j}}\begin{vmatrix} v^{k+1/2}_{i+1/2,j} & w^{k+1/2}_{i+1/2,j} \\ Y^{k+1}_{i,j} & Z^{k+1}_{i,j} \end{vmatrix}.$$

(iii) Use (14) to update $\mathbf{E}_{i,j}$ and advance by one step. At this stage, one only performs the updating of e_3, e_4, and e_5, since there is no need to update the constants e_1 and e_2; while $e_6, e_7, ..., e_{11}$, being identical to U, V, W, X, Y, and Z, have been computed in the previous step.

(iv) Decode $\mathbf{E}^{k+1}_{i,j}$ to obtain $\mathbf{Q}^{k+1}_{i,j}$. For simplicity, all the i, j, k superscripts and subscripts are dropped off. Define

$$A = \frac{(1+\gamma)}{(1-\gamma)}(J^2_{11} + J^2_{12} + J^2_{13}),$$

$$B = \frac{2}{(\gamma-1)}(J_{11}e_3 + J_{12}e_4 + J_{13}e_5),$$

$$C = e_3^2 + e_4^2 + e_5^2 - 2K^2H,$$

where the cofactors are

$$J_{11} = \begin{vmatrix} V & W \\ Y & Z \end{vmatrix}, \quad J_{12} = \begin{vmatrix} U & W \\ X & Z \end{vmatrix}, \quad J_{13} = \begin{vmatrix} U & V \\ X & Y \end{vmatrix}.$$

Then the pressure p satisfies the quadratic equation

$$Ap^2 + Bp + C = 0.$$

It can be shown that $\Delta = B^2 - 4AC \geqslant 0$ and the physically relevant solution for p is

$$p = \frac{-B + \sqrt{\Delta}}{2A}, \tag{22a}$$

and the other flow variables follow directly:

$$u = \frac{e_3 - pJ_{11}}{K}, \quad v = \frac{e_4 - pJ_{12}}{K}, \quad w = \frac{e_5 - pJ_{13}}{K}, \tag{22b}$$

$$\rho = \frac{K}{(J_{11}u + J_{12}v + J_{13}w)}. \tag{22c}$$

(v) Generate grid points (coordinates of cell centers) along streamlines and complete the procedure of marching forward by one step:

$$x_{i,j}^{k+1} = x_{i,j}^{k} + \frac{1}{2}\Delta\lambda^k\left(\frac{u_{i,j}^k}{q_{i,j}^k} + \frac{u_{i,j}^{k+1}}{q_{i,j}^{k+1}}\right),$$

$$y_{i,j}^{k+1} = y_{i,j}^{k} + \frac{1}{2}\Delta\lambda^k\left(\frac{v_{i,j}^k}{q_{i,j}^k} + \frac{v_{i,j}^{k+1}}{q_{i,j}^{k+1}}\right),$$

$$z_{i,j}^{k+1} = z_{i,j}^{k} + \frac{1}{2}\Delta\lambda^k\left(\frac{w_{i,j}^k}{q_{i,j}^k} + \frac{w_{i,j}^{k+1}}{q_{i,j}^{k+1}}\right),$$

$$i = 1, 2, \ldots, m; \quad j = 1, 2, \ldots, n.$$

These relations represent simple trapezoidal integrations along streamlines.

The present step is not a standard Godunov procedure but is unique to the Lagrangian method. By this way, a three-dimensional mesh is automatically generated along the streamlines. Each grid point represents the center of a fluid particle (a computational cell).

Now we complete the numerical procedure for one space step. To march forward further, one goes back to (ii) and repeats (ii)–(v).

3.2. *Application of the TVD scheme*

It is well known that, due to the presence of numerical viscosity, the first-order Godunov scheme strongly smears a discontinuity. In order to improve accuracy, various efforts were made in the past decade to develop high resolution monotonicity-preserving schemes, such as TVD, ENO schemes. Among these, we describe a postprocessing scheme—Sweby's TVD scheme and a preprocessing scheme—Van Leer's MUSCL scheme.

Sweby's TVD scheme procedure [8], which adds limited anti-diffusive terms to the first-order Godunov scheme, is straightforward and convenient. With the results from the Godunov scheme, the **E** vector is upgrated in a component by component way before it is decoded to give new flow variables **Q** in the above Godunov procedure. Following Sweby [8] we apply a flux limiter function ϕ and rewrite (13) in the form

$$\begin{aligned}\mathbf{E}_{i,j}^{k+1} = \mathbf{E}_{i,j}^{k} &- \mu\Delta_-^{\xi}[\mathbf{F}^{\mathbf{G}}]_{i+1/2,j}^{k+1/2} - \kappa\Delta_-^{\eta}[\mathbf{G}^{\mathbf{G}}]_{i,j+1/2}^{k+1/2} \\ &- \mu\Delta_-^{\xi}[\phi(r_i^+)\,\alpha_{i+1/2}^+[\Delta\mathbf{F}_{i+1/2,j}]^+ \\ &- \phi(r_{i+1}^-)\,\alpha_{i+1/2}^-[\Delta\mathbf{F}_{i+1/2,j}]^-] \\ &- \kappa\Delta_-^{\eta}[\phi(s_j^+)\,\beta_{j+1/2}^+[\Delta\mathbf{G}_{i,j+1/2}]^+ \\ &- \phi(s_{j+1}^-)\,\beta_{j+1/2}^-[\Delta\mathbf{G}_{i,j+1/2}]^-], \end{aligned} \tag{23}$$

where $\mu = \Delta\lambda^k/\Delta\xi_i$, $\kappa = \Delta\lambda^k/\Delta\eta_j$, and the superscript **G** stands for the numerical fluxes of Godunov scheme. For any vector **H** the backward difference operators are

$$\Delta_-^{\xi}[\mathbf{H}_{i+1/2,j}] = \mathbf{H}_{i+1/2,j} - \mathbf{H}_{i-1/2,j},$$

$$\Delta_-^{\eta}[\mathbf{H}_{i,j+1/2}] = \mathbf{H}_{i,j+1/2} - \mathbf{H}_{i,j-1/2}.$$

The notation associated with the ξ-fluxes is

$$[\Delta\mathbf{F}_{i+1/2,j}]^+ = \mathbf{F}(\mathbf{Q}_{i+1,j}^k) - \mathbf{F}^{\mathbf{G}_{i+1/2,j}^{k+1/2}},$$

$$[\Delta F_{i+1/2,j}]^- = \mathbf{F}^{\mathbf{G}_{i+1/2,j}^{k+1/2}} - \mathbf{F}(\mathbf{Q}_{i,j}^k),$$

$$\alpha_{i+1/2}^{\pm} = \tfrac{1}{2}[1 \mp v_{i+1/2}^{\pm}],$$

$$v_{i+1/2}^{\pm} = \frac{\mu[\Delta(f_l)_{i+1/2,j}]^{\pm}}{[(e_l)_{i+1,j}^k - (e_l)_{i,j}^k]},$$

$$r_i^{\pm} = \left[\frac{\alpha_{i-1/2}^{\pm}(\Delta(f_l)_{i-1/2})^{\pm}}{\alpha_{i+1/2}^{\pm}(\Delta(f_l)_{i+1/2})^{\pm}}\right]^{\pm 1}.$$

Similarly for the η-fluxes, we have

$$[\Delta\mathbf{G}_{i,j+1/2}]^+ = \mathbf{G}(\mathbf{Q}_{i,j+1}^k) - \mathbf{G}^{\mathbf{G}_{i,j+1/2}^{k+1/2}},$$

$$[\Delta\mathbf{G}_{i,j+1/2}]^- = \mathbf{G}^{\mathbf{G}_{i,j+1/2}^{k+1/2}} - \mathbf{G}(\mathbf{Q}_{i,j}^k),$$

$$\beta_{j+1/2}^{\pm} = \tfrac{1}{2}[1 \mp \omega_{j+1/2}^{\pm}],$$

$$\omega_{j+1/2}^{\pm} = \frac{\kappa[\Delta(g_l)_{i,j+1/2}]^{\pm}}{[(e_l)_{i,j+1}^k - (e_l)_{i,j}^k]},$$

$$s_j^{\pm} = \left[\frac{\beta_{j-1/2}^{\pm}(\Delta(g_l)_{j-1/2})^{\pm}}{\beta_{j+1/2}^{\pm}(\Delta(g_l)_{j+1/2})^{\pm}}\right]^{\pm 1}.$$

Here, e_l, f_l, and g_l are respectively components of **E**, **F**, and **G**, with $l = 3, 4, \ldots, 11$ as their index number. We note that since $e_1 = K$, $e_2 = H$ are constant for all λ along a streamline, the upgrading of the numerical procedure needs to be done for $e_3, e_4, e_5, \ldots, e_{11}$ only. The Van Leer limiter function

$$\phi(r) = \begin{cases} 0, & r < 0, \\ \dfrac{2r}{r+1}, & r > 0, \end{cases} \tag{24}$$

is employed throughout this paper, since it was found [13] that there is no substantial difference in the numerical results between applying different limiter functions.

When the vector **E** is upgraded by the high resolution TVD scheme, one may follow step by step the same procedure as in the Godunov scheme.

In the preprocessing MUSCL scheme, the upgrading is carried out for the flow variables u, v, w, p, and ρ before they are applied as the input for the local Riemann solvers. The upgrading is performed in a dimension-by-dimension way. For example, in the ξ direction, let f be any of the above physical variables, then, instead of assuming a uniform state

in the cells (i, j) and $(i+1, j)$, we assume linearly distributed states and use the linear relation to determine cell interface flow variables and use them as the input to the local Riemann solver,

$$f_t = f_{i+1,j} - 0.5(f_{i+2,j} - f_{i+1,j})\,\phi(r^+),$$
$$r^+ = \frac{f_{i+1,j} - f_{i,j}}{f_{i+2,j} - f_{i+1,j}},$$
$$f_b = f_{i,j} + 0.5(f_{i,j} - f_{i-1,j})\,\phi(r^-),$$
$$r^- = \frac{f_{i+1,j} - f_{i,j}}{f_{i,j} - f_{i-1,j}},$$

where

$$\phi(r) = \max(0, \min(1, r))$$

is the minmod flux limiter and t and b correspond to top and bottom states. These new f_t and f_b are then fed to the local pseudo 3D Riemann solvers; the rest of the procedure will be the same as the Godunov one described in Section 3.1.

The TVD schemes lead to better accuracy in the continuous region and higher resolution across discontinuities, as will be seen in Section 6.

4. SOLUTION OF THE PSEUDO THREE-DIMENSIONAL RIEMANN PROBLEM

As a building block, the Riemann problem and its solution play an important role in the Godunov-type schemes in the numerical solution of inviscid compressible perfect gas flow problems. According to the Godunov scheme, a three-dimensional Riemann solver is required in our numerical procedure (Fig. 2a). As we pointed out earlier, the exact solution to a general three-dimensional Riemann problem is not yet known. Even if it were available, the procedure must be rather complicated and lack of efficiency. Chang and Zheng [10] have a detailed description of the complexity of the higher dimensional Riemann problem. A practical remedy is to employ the idea of the dimensional splitting. The dimension-splitting technique reduces the number of initial constant states from four in the full three-dimensional Riemann problem to two in the so-called pseudo three-dimensional Riemann problem (Fig. 2b). This amounts to replacing the exact but unavailable three-dimensional Riemann problem solution by four approximate ones that are already known. In this section, we will study the pseudo three-dimensional Riemann problem (PRP) and its solution, discuss its validity as as approximation to the 3D Riemann problem in the dimension-splitting technique, and then, as a consequence, show why the new Lagrangian approach leads to crisp resolution of contact discontinuity (slip surface).

Given two uniform states $\mathbf{Q}_t$ (top state) and $\mathbf{Q}_b$ (bottom state) in a three-dimensional space, we assume that the two states are separated by a plane and that the direction of the interaction line is known by referring to the above section and Figs. 2b and c. As in Fig. 3, we choose the direction of interaction line as the z-direction and the plane that separates $\mathbf{Q}_t$ and $\mathbf{Q}_b$ (separating plane) as the y-z coordinate plane. Then we have a Cartesian x-y-z coordinate system. In this system the Euler equations for three-dimensional steady flow have the form

$$\begin{aligned}
&\frac{\partial(\rho u)}{\partial x} + \frac{\partial(\rho v)}{\partial y} + \frac{\partial(\rho w)}{\partial z} = 0 \\
&u\frac{\partial u}{\partial x} + v\frac{\partial u}{\partial y} + w\frac{\partial u}{\partial z} + \frac{1}{\rho}\frac{\partial p}{\partial x} = 0 \\
&u\frac{\partial v}{\partial x} + v\frac{\partial v}{\partial y} + w\frac{\partial v}{\partial z} + \frac{1}{\rho}\frac{\partial p}{\partial y} = 0 \\
&u\frac{\partial w}{\partial x} + v\frac{\partial w}{\partial y} + w\frac{\partial w}{\partial z} + \frac{1}{\rho}\frac{\partial p}{\partial z} = 0 \\
&u\frac{\partial}{\partial x}(p/\rho^\gamma) + v\frac{\partial}{\partial y}(p/\rho^\gamma) + w\frac{\partial}{\partial z}(p/\rho^\gamma) = 0,
\end{aligned} \tag{25}$$

where u, v, w, p, and ρ are respectively the velocity components in the new Cartesian coordinate system, pressure and density. Let the two given states be written as

$$\begin{aligned}
&\mathbf{Q}_t = (u_t, v_t, w_t, p_t, \rho_t)^{\mathrm{T}}, \qquad x > 0, \\
&\mathbf{Q}_b = (u_b, v_b, w_b, p_b, \rho_b)^{\mathrm{T}}, \qquad x < 0,
\end{aligned} \tag{26a}$$

and

$$\partial/\partial z = 0, \qquad \text{and} \qquad w = \text{const.} \tag{26b}$$

Equation (25) is reduced to the Euler equations of two-dimensional steady flow:

$$\begin{aligned}
&\frac{\partial(\rho u)}{\partial x} + \frac{\partial(\rho v)}{\partial y} = 0, \\
&u\frac{\partial u}{\partial x} + v\frac{\partial u}{\partial y} + \frac{1}{\rho}\frac{\partial p}{\partial x} = 0, \\
&u\frac{\partial v}{\partial x} + v\frac{\partial v}{\partial y} + \frac{1}{\rho}\frac{\partial p}{\partial y} = 0, \\
&u\frac{\partial}{\partial x}(p/\rho^\gamma) + v\frac{\partial}{\partial y}(p/\rho^\gamma) = 0.
\end{aligned} \tag{27}$$

The condition (26a), assuming that two uniform flows separated by a plane and the direction of interaction line are given, together with the condition (26b) stating that the two

flows are uniform in the z-direction either before or after the interaction, are generally satisfied in our Godunov scheme above. This ensures our using the 2D system (27) to replace the local 3D system (25).

Now we consider the two-dimensional Riemann problem of (27) with the initial condition (Fig. 3),

$$\mathbf{Q}^0 = \begin{cases} \mathbf{Q}_t^0, & x > 0, \\ \mathbf{Q}_b^0, & x < 0, \end{cases} \tag{28}$$

where $\mathbf{Q}^0 = (u, v, p, \rho)^T$, $\mathbf{Q}_t^0 = (u_t, v_t, p_t, \rho_t)^T$, and $\mathbf{Q}_b^0 = (u_b, v_b, p_b, \rho_b)^T$. This is a standard two-dimensional Riemann problem and can be solved based on (27) and the Rankine–Hugoniot relations by Newton's iteration. The solution, which we still denote by $\mathbf{Q}^0$, generally consists of all the elementary waves, namely, the oblique shock, the slipline, and the Prandtl–Meyer expansion. Based on $\mathbf{Q}^0$, we construct the Riemann solution of (25) as

$$\mathbf{Q} = \begin{cases} (u, v, w_t, p, \rho)^T, & x > x_s, \\ (u, v, w_b, p, \rho)^T, & x < x_s, \end{cases} \tag{29}$$

where x_s is the x-coordinate of the slip surface.

Since $\partial \mathbf{Q}/\partial z = 0$ and w_t, w_b are given constants, the conditions of (26) are satisfied. Therefore, (29) is the solution of (25) and hence, the name of "pseudo three-dimensional Riemann problem solution." Physically $\mathbf{Q}$ may be regarded as translating along the z direction, the upper part (the part above the slip surface) and the lower part (the part below the slip surface) of $\mathbf{Q}^0$ at different speeds (w_t and w_b) across the slip-surface. A numerical example will be illustrated in Section 6.

If a solid boundary is present, only one initial state, say, $\mathbf{Q}_t$ is considered in the pseudo three-dimensional Riemann problem (Fig. 2d). The problem is now termed a pseudo three-dimensional boundary Riemann problem (PBRP). Similar to the above procedure, we first solve the corresponding two-dimensional boundary Riemann problem and obtain the solution $\mathbf{Q}^0 = (u, v, p, \rho)^T$ and let $\mathbf{Q} = (u, v, w_t, p, \rho)^T$; then $\mathbf{Q}$ is the solution of the pseudo boundary Riemann problem since (26) is satisfied.

Next in this section, for completeness, we briefly describe the solution of the 2D Riemann problem and 2D boundary Riemann problem. The procedure is the same as in [4] and more details can be found from there.

It should be noted that even an exact 2D Riemann solution is sought and applied to the 3D problem; the final solution is still an approximate one due to other approximations. As in the case of Eulerian approach, the exact Riemann solver may not be really needed and approximate Riemann solvers or flux-splitting methods are considered to be applicable. The use of the approximate Riemann solvers or flux splittings may prove to be effective and can greatly save CPU time in practical computations. This subject is beyond the scope of the current paper and can be a topic of future research. Nevertheless, the exact 2D Riemann solver is still employed in the present work. We also warn that the 2D Riemann solver does not always have a solution. As this situation occurs, the supersonic marching scheme fails.

As an analogue to the one-dimensional Riemann problem for unsteady flow, the standard Riemann problem for two-dimensional steady flow is an initial value problem of the system (27) with a discontinuous initial condition (28),

$$\mathbf{Q} = (u, v, p, \rho)^T = \begin{cases} \mathbf{Q}_t, & x > 0, \\ \mathbf{Q}_b, & x < 0, \end{cases} \tag{30}$$

where the subscripts t and b denote respectively top and bottom states (Fig. 3b), which are counterparts to the left and right states in one-dimensional unsteady flow. For brevity, the superscript "0" has been dropped.

The solution of the 2D Riemann problem is self-similar in the variable y/x and consists of three types of elementary waves, namely, the oblique shock (+), the Prandtl–Meyer expansion (−) and the slipline (0) (Fig. 3).

Let $\mathbf{Q}_0 = (u_0, v_0, p_0, \rho_0)^T$ and $\mathbf{Q} = (u, v, p, \rho)^T$ be the states across one of the above +, −, and 0 elementary waves and $\alpha = p/p_0$. Then, through any state $\mathbf{Q}_0$, with p as parameter, there are two families of state connecting to $\mathbf{Q}_0$, namely, the compression states ($p \geqslant p_0$, $\alpha \geqslant 1$) and the expansion states ($p \leqslant p_0$, $\alpha \leqslant 1$). The two families join smoothly at $\mathbf{Q}_0$ and can be regarded as a single family. This makes it possible to apply Newton's iterative procedure in the solution of the Riemann problem. The center issue in the

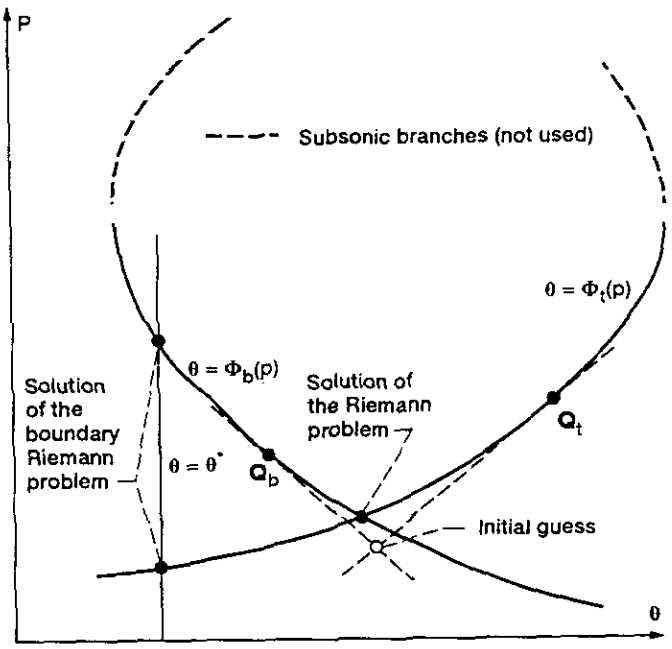

FIG. 4. Solution of 2D Riemann problem.

solution procedure is to find common values of p and θ (p^*, θ^*) at the slipline (Fig. 4). We now illustrate the solution details:

(i) In the $p-\theta$ plane (Fig. 4), there are two curves passing through the two given states $\mathbf{Q}_0 = \mathbf{Q}_t$ and $\mathbf{Q}_0 = \mathbf{Q}_b$. They are respectively defined as

$$\theta = \Phi_t(p) = \begin{cases} \theta_t + \tan^{-1} \\ \quad \left[\dfrac{\alpha-1}{\gamma M_t^2 - \alpha + 1}\left(\dfrac{2\gamma M_t^2}{(\gamma+1)\alpha+\gamma-1} - 1\right)^{1/2}\right], \\ \quad p \geqslant p_t, \\ \theta_t + \nu(M_t) - \nu(M), \qquad p \leqslant p_t, \end{cases} \tag{31a}$$

and

$$\theta = \Phi_b(p) = \begin{cases} \theta_b + \tan^{-1} \\ \quad \left[\dfrac{\alpha-1}{\gamma M_b^2 - \alpha + 1}\left(\dfrac{2\gamma M_b^2}{(\gamma+1)\alpha+\gamma-1} - 1\right)^{1/2}\right], \\ \quad p \geqslant p_b, \\ \theta_b + \nu(M_t) - \nu(M), \qquad p \leqslant p_b, \end{cases} \tag{31b}$$

where $\nu(M)$ is the well-known Prandtl–Meyer function. These curves are sketched in Fig. 4.

(ii) The Newton iterative procedure is then employed to find the intersect (p^*, θ^*) of the two curves. The object function to be driven to zero in the Newton procedure is

$$f(p) = \Phi_t(p) - \Phi_b(p) \tag{32}$$

and the intersect of the tangent lines passing through $\mathbf{Q}_t$ and $\mathbf{Q}_b$ is used as an initial guess to the solution. In practice we use the numerical derivative to replace the analytical ones. Usually it takes 2–4 iterations to converge to a tolerance of $\varepsilon \leqslant 10^{-6}$.

(iii) With the slipline values (p^*, θ^*) calculated, we evaluate the new ρ on either side across the slipline by the Hugoniot relation,

$$\rho = \begin{cases} \rho_0 \left[\dfrac{(\gamma+1)\alpha+\gamma-1}{(\gamma-1)\alpha+\gamma+1}\right], & \alpha \geqslant 1, \\ \rho_0 \alpha^{1/\gamma}, & \alpha < 1; \end{cases} \tag{33}$$

then the speed q via the total enthalpy H of the corresponding cell. Finally, the velocity components are available by

$$u = q\cos\theta^*, \qquad v = q\sin\theta^*. \tag{34}$$

These newly calculated flow variables u, v, p^*, and ρ represent the state at the slipline. Recall that in our Lagrangian formulation a slip-surface coincides with the cell interface (a stream surface); these data are directly employed to calculate cell interface fluxes as we described in the previous section.

At the solid boundary, the flow inclination condition is imposed and one of the curves in the p-θ plane, say, $\theta = \Phi_b(p)$ degenerates to a straight line $\theta = \theta^* = \text{const}$ parallel to the p axis (Fig. 4). In [4], this particular problem is termed "boundary Riemann problem." The solution of a boundary Riemann problem is similar to the above procedure, except by using a different object function,

$$f(p) = \Phi_t(p) - \theta^* \qquad \text{or} \qquad f(p) = \Phi_b(p) - \theta^*.$$

At this stage, we are able to show that, as a result of the application of the Riemann solution and the Godunov scheme to the new Lagrangian formulation, the slip surface (contact discontinuity) resolution remains sharp all the time. The rest of the section will be devoted to this topic.

Consider a typical case that a slip surface exists between two continuous flows and coincides with the cell interfaces between cells $(i+1, j)$ and (i, j), $j = 1, 2, \ldots, n$. Thus,

$$p^k_{i+1,j} = p^k_{i,j}$$

and both $\mathbf{V}^k_{i+1,j}$ and $\mathbf{V}^k_{i,j}$ are parallel to the cell interfaces, while there are jumps in ρ and the flow speed $q = |\mathbf{V}|$. In the marching, after interaction of the two flows, since the new cell interface follows exactly the new slip-surface (a steam surface), the above relation still holds at the new cell interface. Then the cell interface flux $\mathbf{F}^{k+1/2}_{i+1/2,j}$ on either side of the slip surface is *continuous* on the very same side where it is derived, and still produces *continuous solutions* through the Godunov scheme along each side of the slip surface. The pressure is continuous in the whole region since it is continuous across the slip surface. On the other hand, the original discontinuities in ρ and q across the slip surface will still remain there since the marching evolution on each side of the slip surface is continuous. In other words, the slip surface remains sharp during the marching. In a special case that both continuous flows are uniform, it is easily seen from the Godunov scheme that both flows remain unchanged during the marching forward.

In the case the slip surface does not coincide with a cell interface, say, when it is generated by shock interaction, the cell through which the true slip surface passes will be considered as one of the intermediate cells in the captured slip surface. Based on the above argument, no more intermediate cells will be generated around the true slip surface, i.e., no further smearing will occur during the marching. Moreover, application of a high resolution TVD scheme

(such as the Sweby's) will help to reduce the number of the intermediate cells and render a sharper captured slip surface.

In the new 3D Lagrangian approach, the resolution of slip surface is similar to its 2D counterpart, as has been described by Hui and Loh [13]. Comparing to the ever smearing and deteriorating resolution of contact discontinuity in the Eulerian formulation, the new Lagrangian approach has, indeed, provided an excellent attack to the important issue. In the last numerical example in Section 6, a comparison between results from the Eulerian approach and the new Lagrangian approach is presented.

5. WELL-POSEDNESS OF THE CAUCHY PROBLEM IN GAS DYNAMICS AND ITS NUMERICAL TREATMENT

For a supersonic flow of Mach number $M > 1$ everywhere, the Euler equations of gas dynamics, either in Eulerian or Lagrangian formulation, are of hyperbolic type (see the Appendix). The numerical solution marches

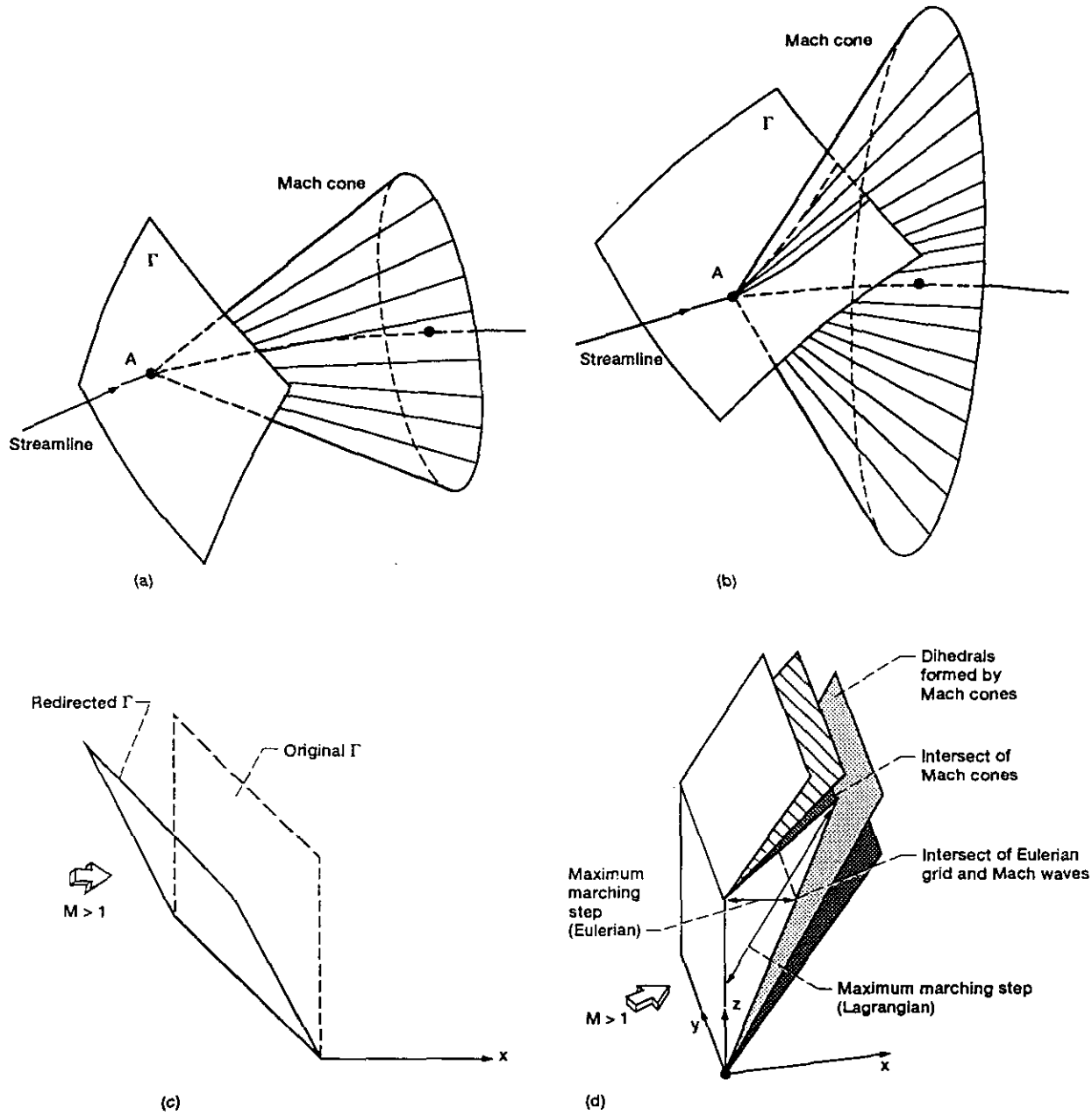

FIG. 5. Well-posedness of the Cauchy problem: (a) Γ lies upstream of Mach cone; (b) Γ turns into Mach cone; (c) example of Γ redirection; (d) Lagrangian Courant number could be larger than the Eulerian one.

forward along a time-like direction, say, the x-direction in the Eulerian formulation or the flow direction (τ or λ) in the new Lagrangian formulation. In any case, the well-known CFL condition rules the maximum marching step size in order to maintain stability.

Another important factor that controls the numerical stability is the well-posedness of the Cauchy problem (initial problem) of the Euler equations. The well-posedness may be regarded as a general CFL condition. If it is violated, the numerical procedure will soon blow up. The property of the new Lagrangian system (13) that the physical flow is closely followed makes the well-posedness analysis very intuitive and straightforward. Consider a computational cell (also a fluid particle) in Fig. 5, where the initial data are given on the time (distance) surface Γ. For the well-posedness of this local Cauchy problem of (13), the basic theory of hyperbolic equation (see Courant and Hilbert [14]) stipulates that Γ must lie upstream of the domains of influence (i.e., the Mach cones) issuing from every point of Γ; in particular, those Mach cones issuing from the vertices of Γ.

When a supersonic flow passes through a strong shock, similar to the 2D case [15], the Mach number drops down and the Mach cones downstream of the shock expand to wider angles, while Γ changes its inclination as well (this is more pronounced in the τ-conservation form). It is possible that at some marching step, the surface Γ extends into the interior of the Mach cone (Fig. 5b) and renders the local Cauchy problem ill-posed. Following the experience from the 2D version [15], a remedy is to redirect the inclination (direction of normal vector) of the initial time (distance) surface of each cell so that even after the flow passes through the shock, the time surface still lies upstream of the Mach cones. Due to the flexibility of time (distance) surface, the redirection procedure can be performed not only at the initiation stage but also in the midst of the computation, without disturbing the formulation and any data already computed.

The same difficulty o well-posedness, of course, exists in the Eulerian formulation as well. However, as a result of the fixed time-like marching direction, say, the x-direction, one has to artificially rotate the reference frame and perform all the pertinent coordinate transformations. Marconi and Moretti [16] have used this approach. They employ a local coordinate rotation to their non-conservative implicit shock-fitting scheme to assure the proper domain of dependence of the grid points so that supersonic velocity in the marching direction is maintained. For a conservative shock-capturing scheme, the procedure is expected to be even more cumbersome. In this regard, the Lagrangian formulation is much easier than the Eulerian ones; we simply redirect the time (distance) surface.

In addition, as in the 2D case [15], it is interesting and worth pointing out another advantage of the new Lagrangian formulation over its Eulerian counterpart: the scheme may march forward with a larger Courant number. This situation is illustrated in Fig. 5d, assuming that the initial surface coincides with the x-y plane. Due to the complexity of three dimensional geometry, we only present a section of the entire configuration; it is still seen that the Lagrangian formulation appears to have an "optimal" Courant number since its marching direction (the flow direction) is right in the middle of the Mach cones; while the maximum Eulerian marching step in the fixed x-direction is not to exceed where the Eulerian cell interface intersects any Mach wave.

6. TEST PROBLEMS

In order to test the accuracy and robustness of the new three-dimensional Lagrangian method, we apply it to several test examples and compare the results to the exact solutions, existing numerical solutions or experimental results whenever they are available.

The first example is a pseudo three-dimensional Riemann problem. Two flows with states $\mathbf{Q}_1$ and $\mathbf{Q}_2$ as described in Fig. 6 are separated by the separating plane and begin to interact with each other at the interacting line, see Fig. 6a. The problem is analysed in Section 4 and the exact solution can be easily obtained via a standard two-dimensional Riemann solver. In Figs. 6b and c, we illustrate the pressure and density distributions along a time surface in the x-y plane (interaction plane). It is observed that both numerical results by Godunov and TVD schemes agree well with the exact solution. In particular, the slipline resolution is so crisp that there is practically no point in between. The TVD scheme produces more accurate results in the continuous part of the flow and a sharper profile across the shock. In this example a mesh of 100×50 (in the y-z plane) cells is employed.

In the second example, we consider a truly three-dimensional initial value–boundary value problem—the supersonic inviscid corner flow. The geometrical configuration is shown in Fig. 7a. Two intersecting wedges, both with angles of 9.5°, form an axial corner over which there is a Mach 3 flow. The flow field consists of two planar wedge shock, two embedded shocks, a corner shock, and the shear layers (slip-surfaces) as shown in Fig. 7. West and Korkegi [17] carried out an experiment for this case, which we intend to use as a comparison to our numerical result. In their experiment, the turbulent boundary layers are thin and their effect on the shock displacement is minimal. Thus, the overall picture may be considered as an inviscid phenomenon, except near the walls. We employ a mesh of 45×45 points in the y-z plane for the computation. We use a 3D color displaying package FAST, developed by NASA Ames Research Center, for presenting the numerical results. But the color pictures are turned into grey ones for convenience.

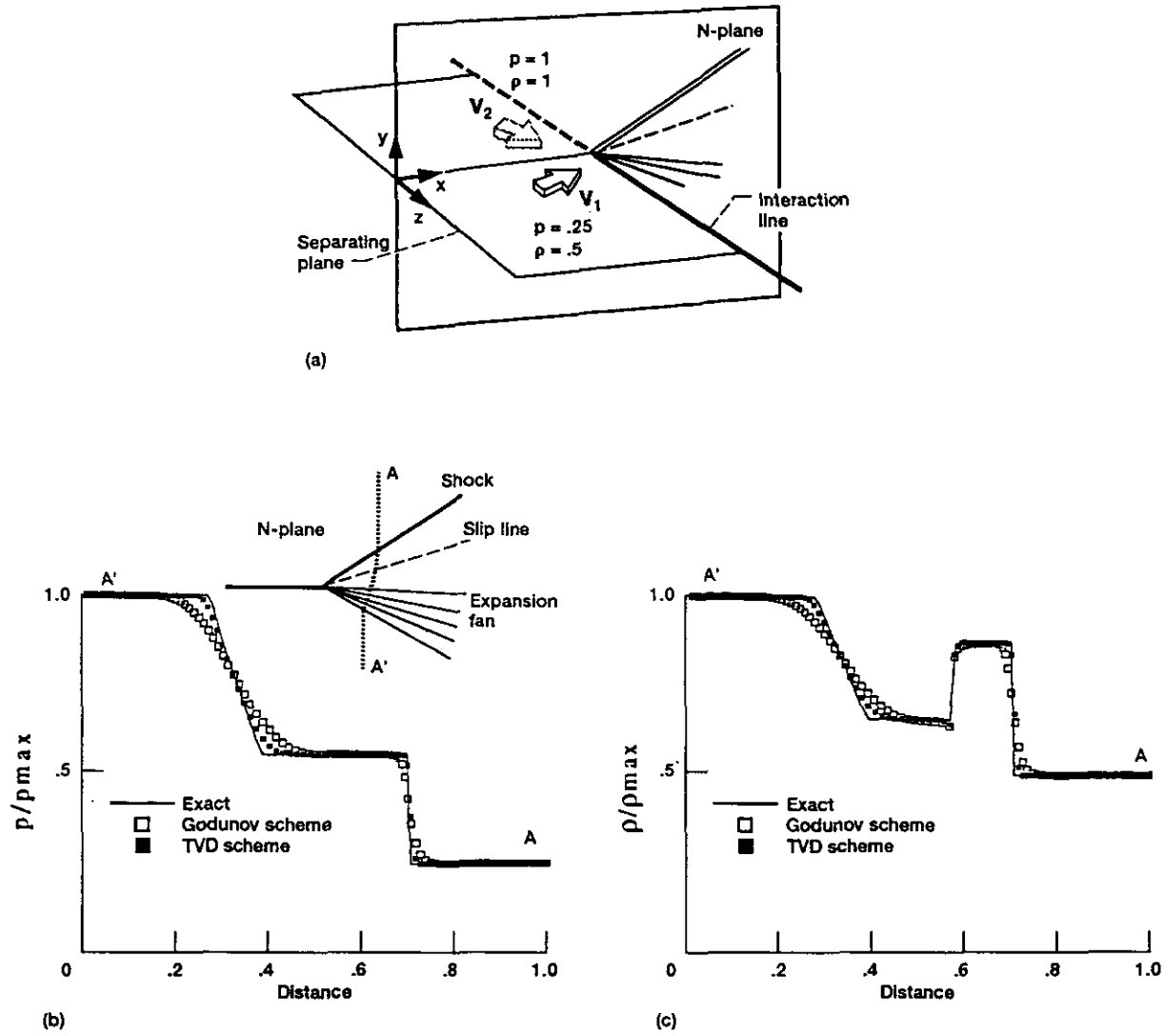

FIG. 6. A pseudo 3D Riemann problem: (a) numerical solutions on plane $N(x\text{-}y$ plane). $\mathbf{V}_1 = (3.3466, 0, -1)$ for $y > 0$, $\mathbf{V}_2 = (2.8397, 0, 0.8)$ for $y < 0$; (b) pressure distribution along line AA' on N-plane; (c) density distribution along line AA' on N-plane.

Figure 7b illustrates the u-velocity contours on a typical λ plane. The corner shock, embedded shocks, and 2D wedge shocks are clearly shown. In particular, the triangular slip-surfaces are distinct and sharp. They all agree well with the experimental locations by West and Korkegi [17]. In Fig. 7c, we present the isobars on the same λ plane. All the shocks are still clearly visible. The slip-surfaces now disappear because the pressure across them is continuous. However, a gentle decrease in pressure appears from the corner shock toward the walls and the wall corner. Figure 7c shows the isopycnics (density contours) on the same λ-plane. The density peaks at the two triple points, where the embedded shock, the wedge shock, and the corner shock meet one another. Figure 7e displays how the grid on a typical plane deforms with the flow, the grid remains straight until the shock is encountered and changes in conform with the deflection of the streamline. The shock angle agrees well with the exact solution for the 2D wedge shock. Finally, in Fig. 7f, we include the result by Liou and Hsu [18], which is based on solving the Navier–Stokes equations with very high Reynolds number in the standard Eulerian formulation. The similar 45×45 but non-uniform grid points with finer size at the walls are used in their example. It is seen that their slip-surfaces are less clear.

In the third problem, we calculate a Mach 4 flow past a delta wing with a 10° angle of attack. In this case, we intend to show the robustness of our method in handling different body shapes in supersonic flow. The symmetrical wing body is illustrated in Fig. 8a. The semi-span angle $\delta = 40°$, the semi-thickness angle $\phi = 2.5°$ and its longitudinal cross

section is diamond shaped. Initially, the vector **T** is chosen to be the unit vector along the projection of wing edge AC on y-z plane. A total 50×50 mesh is employed in the computation. Figure 8b illustrates the isobars at different stations around the wing body, bow shock at the top, expansion fan at the bottom, and other expansion fans arising from the central ridge and the trailing edge are clearly displayed. Figure 8c shows the isobars on the upper wing body surface (a stream surface). One sees the shock at the leading edge and the expansions at the central ridge and the trailing edge. The little "zigzags" in the contours are due to the non-alignment of the vector **T** with the leading edge or ridge line in

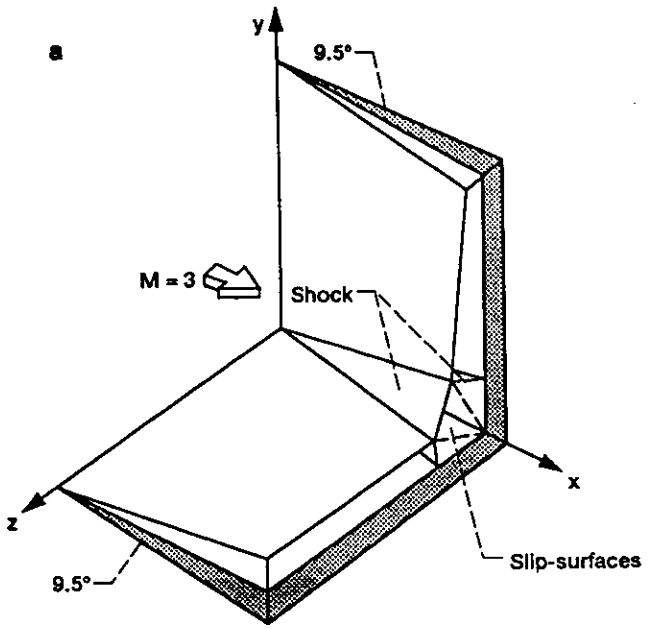

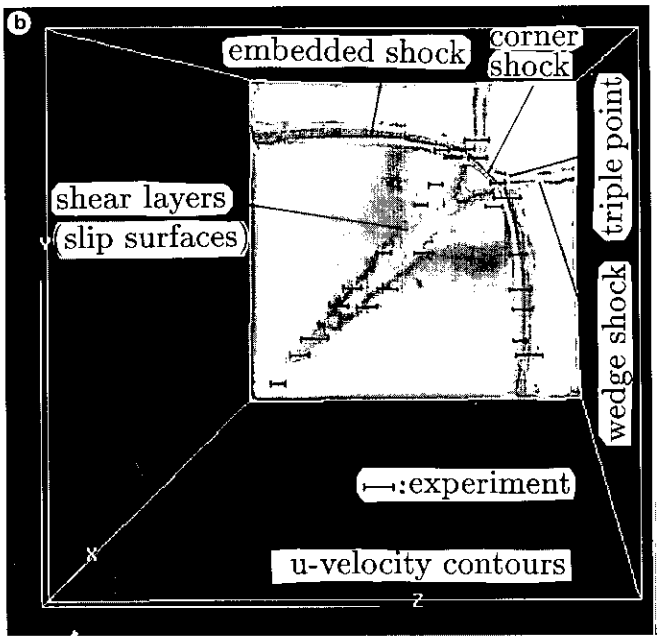

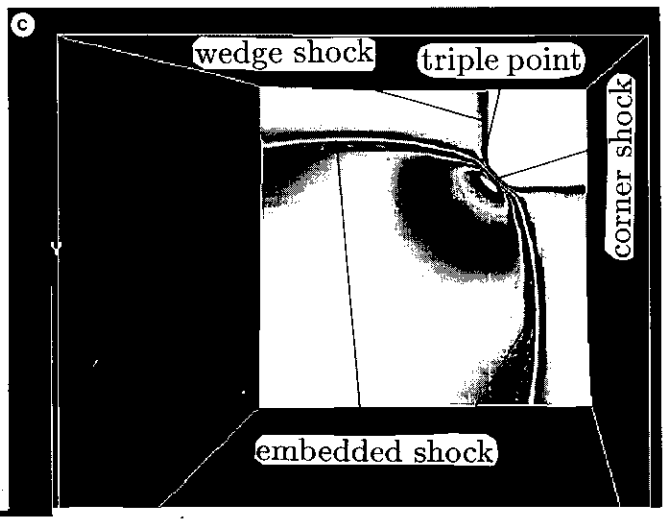

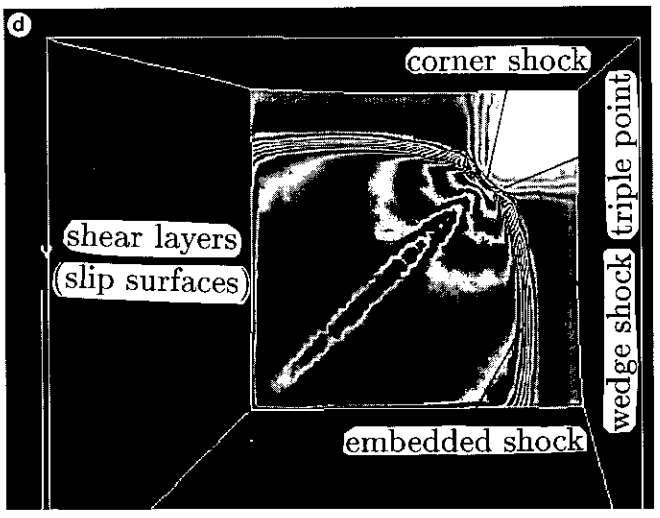

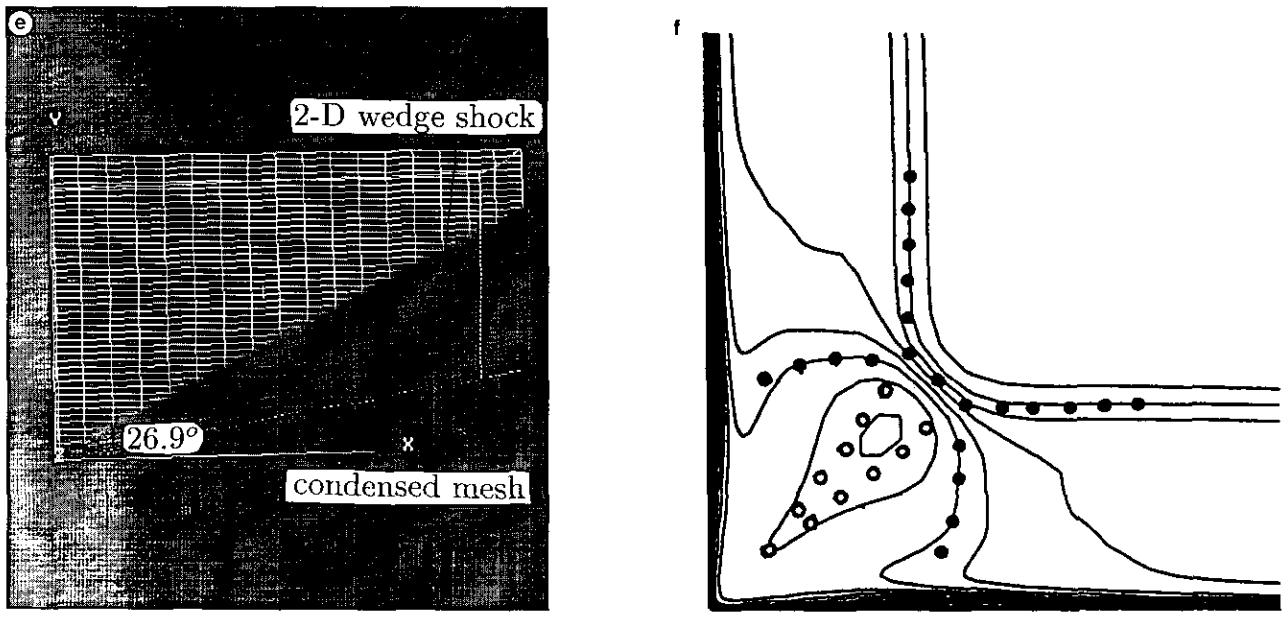

FIG. 7—*Continued*

each cell. For numerical stability reasons, such a choice for **T** is necessary (see Section 4), and the unpleasant "zigzags" soon disappear on other stream surfaces. Figures 8d and e show the isobars on two typical stream surfaces that are parallel to, but above and below, the wing body. In Figs. 8f and g, we demonstrate the isobars and isopycnics on the symmetric plane. Bow shock, trailing shock, three expansion fans, and, in particular, the slipline are clearly displayed. In Fig. 8g, one can even find a very weak wave as a result of the reflection of the ridge fan from the leading-edge shock. Furthermore, in Figs. 8h and i we present the detailed pressure and density distribution along a typical λ line on the symmetric plane to show the quality of the solution, in particular, a clear discontinuity across the slipline (surface) in Fig. 8i. Finally, Figs. 8j and k show the isobars and isopycnics on a typical spanwise cross section parallel to the symmetric plane. They bear features similar to those in the symmetric plane.

In the last example, we compute a novel 3D Riemann problem. For many years, the 3D Riemann problem has been a topic of constant interest and remained unsolved. To our knowledge, we are the first to calculate the numerical solution of a problem of this type. The capability of our scheme is based on its excellent behavior across the slip-surface. Having no existing solution for comparison, we employ grid meshes of 50×50 and 100×100 and confirm that the results are similar. Another confirmation comes about from a side-by-side comparison with the result by an Eulerian finite volume approach (Fig. 10) employing same number of cells. The Riemann problem in question is shown in Fig. 9a, where the initial conditions are given in the four quadrants of the y-z plane. For better understanding of the flow, we choose identical states in the first and third and second and fourth quadrants, that is,

$$\mathbf{Q}_1 = (u_1, v_1, w_1, p_1, \rho_1)^{\mathrm{T}} = (5, 0, 0, 0.25, 0.5)^{\mathrm{T}},$$

$$\mathbf{Q}_2 = (u_2, v_2, w_2, p_2, \rho_2)^{\mathrm{T}} = (3.5, 0, 0, 1, 1)^{\mathrm{T}}.$$

Figure 9b shows the isobars on a typical λ plane where the flow is fully developed. Due to symmetry, only part of the waves are labelled. At the outskirts around the four sides, as expected, the flow behaves like two-dimensional flows with all the 2D elementary waves, namely, shocks, sliplines (surfaces), and Prandtl–Meyer expansion fans. In the interior, genuine 3D flow occurs. A singular point (line) is produced when two 2D shocks collide with each other. This singular point forms the nucleus of a compression kernel. When two 2D expansions come together, they form an expansion kernel. The compresion kernels and expansion kernels are connected by continuous interior flow except across a slip-surface. The compression, expansion kernels, 2D shocks, and expansion fan regions are clearly observed. Similar to the 2D case, between a shock and its corresponding region, their exists a region of uniform pressure. The density contours are presented in Fig. 9c. The slip-surfaces are crisp since they are never smeared by the Lagrangian approach. Figure 9d demonstrates the contours of u-velocity component. In both Figs. 9c and d, the slip-surfaces form a pair of

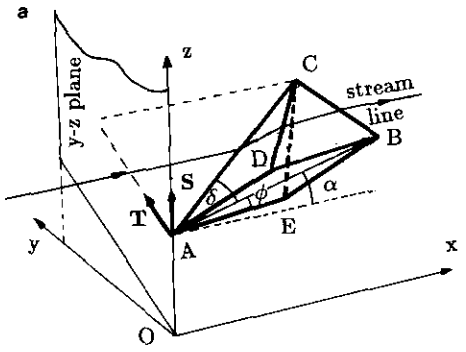
a
y-z plane
z
C
stream
line
B
D
S
T
A
E
y
x
O

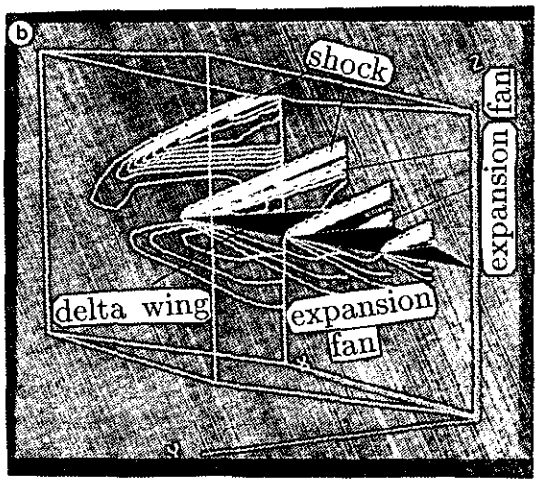
b
shock
fan
expansion
delta wing
expansion
fan

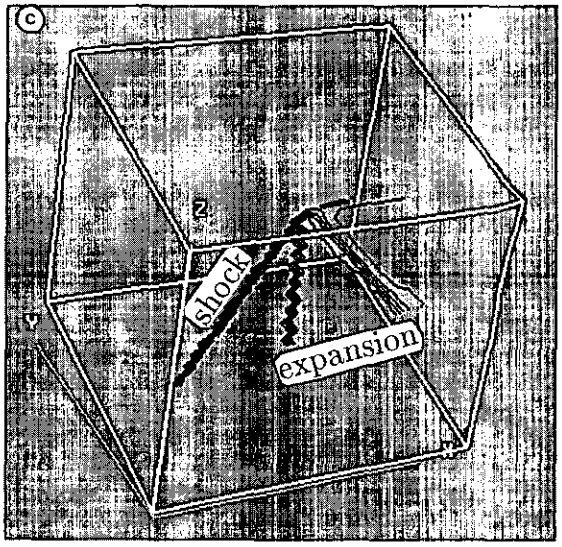
c
shock
expansion

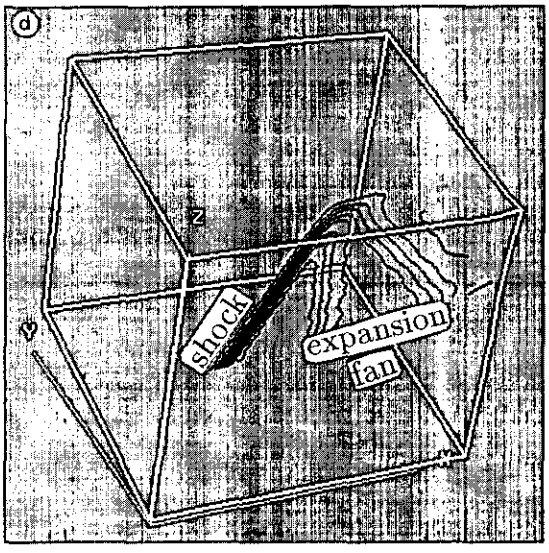
d
shock
expansion
fan

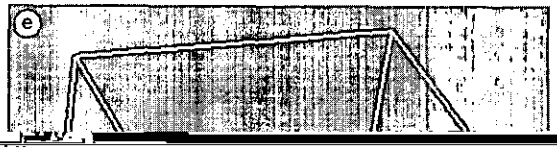
e


f
fan

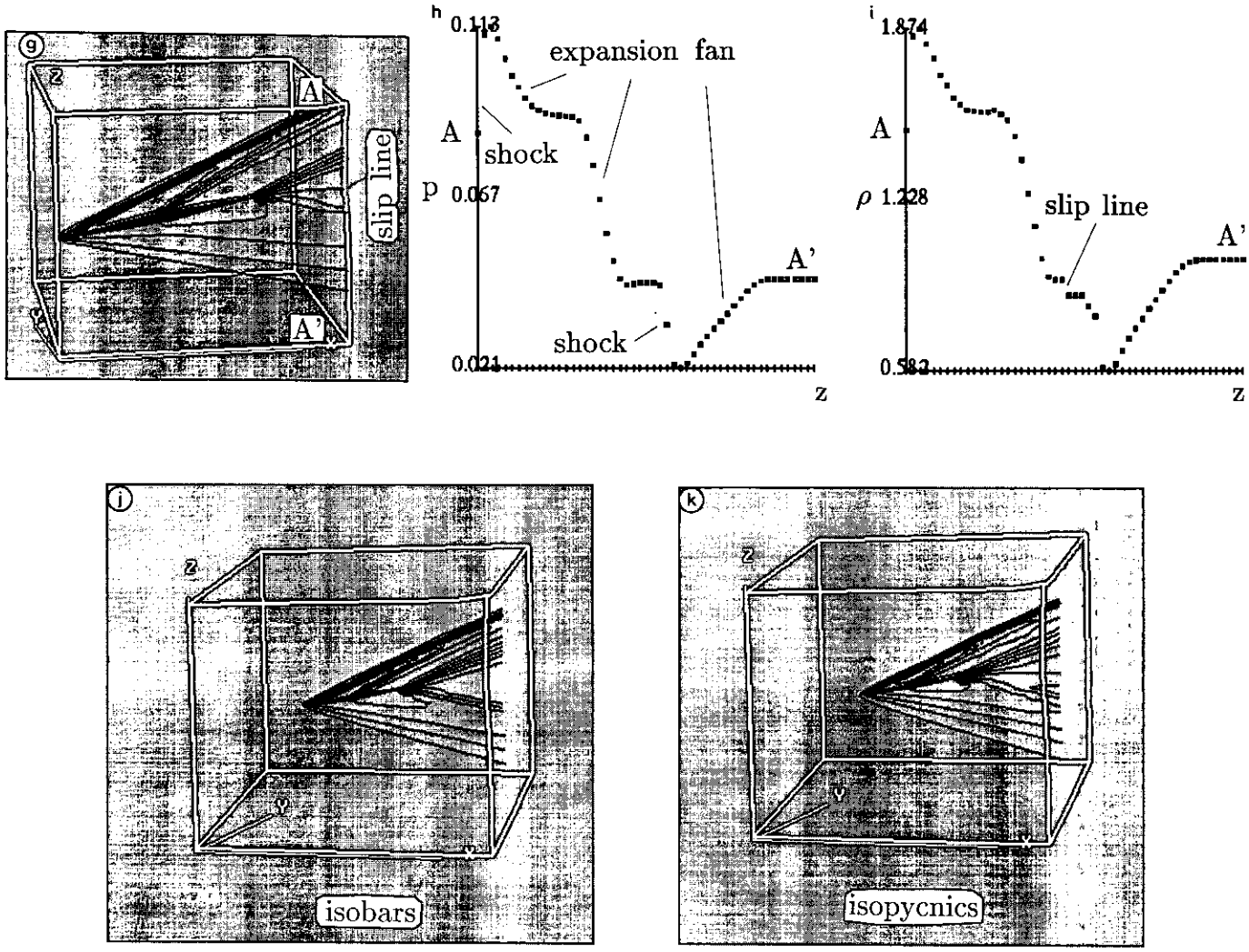

FIG. 8—*Continued*

curved symmetrical surfaces. It is interesting to compare the phenomena at a compression kernel to those of the well-known corner flow problem (Example 2). In a corner flow problem, when the two 2D wedge shocks collide, a new corner shock and two embedded shocks are generated, together with two triple points and a shear layer (slip-surfaces). In the 3D Riemann problem, with the absence of body surfaces, however, the collision of 2D shocks only produces a singular point(line). Around the singular point in the compression kernel, the 2D shocks vanish continuously.

Figure 9e shows a side view of the solution at one of the outermost stream surfaces. On this stream surface, the flow is identical to a 2D Riemann problem solution. In Fig. 9f, we display the shape of a slip-surface and several typical meshes. It is seen that the meshes are automatically deformed, expanded, or condensed, according to the flow. Generally, our result agrees well with the qualitative description in the paper by Chang and Zheng [10].

At last, in Fig. 10, we display contours of constant density and Mach number, resulting from the Eulerian approach at a typical station for a side-by-side comparison with the Lagrangian result. Great care has been taken in constructing the Eulerian formulation to ensure reliable results. For example, the pseudo 3D Riemann solver of Section 4 is employed in this approach to take care of the interaction between two 3D flows across the cell interface, and the effects of 3D flow complexity are respected as much as possible. From the similarity of flowfield patterns, we confirm that both approaches give consistent numerical results. On the other hand, it is observed that the slip-surfaces by the Eulerian approach have grown excessively, such that the flow field pattern is greatly distorted, while the Lagrangian counterparts remain crisp.

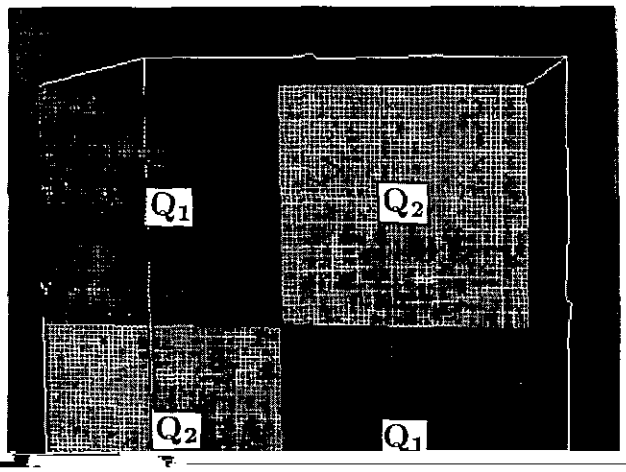

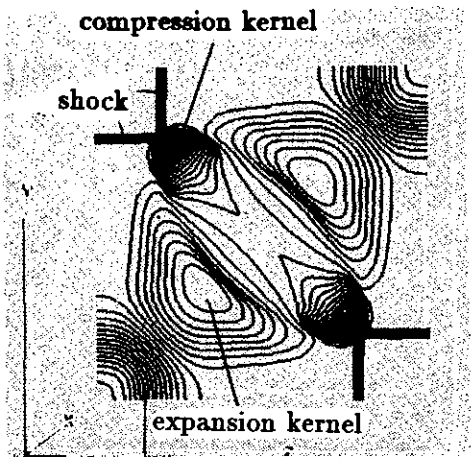

(b)

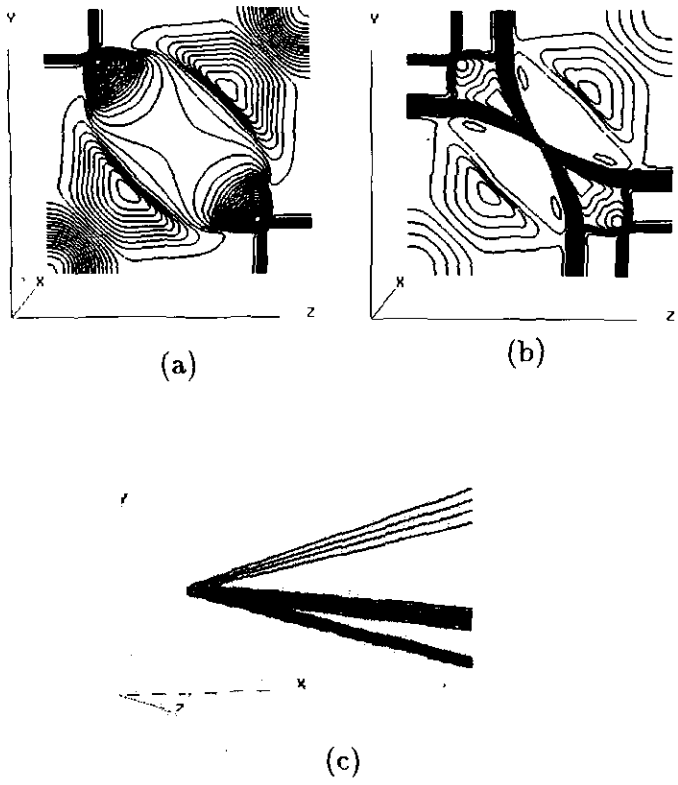

FIG. 10. Solution to the symmetrical 3D Riemann problem by an Eulerian approach for comparison with the Lagrangian one: (a) isobars on a x-plane; (b) isomachs on a x-plane; (c) isomachs on a side plane. Compared to Figs. 9(b), (d), and (e), respectively.

CONCLUDING REMARKS

In this paper, we have developed a new Lagrangian method for steady three-dimensional supersonic flow computation. The method employs the "Lagrangian distance" and the stream functions as the independent variables, in place of the Cartesian coordinates x, y, and z. The boundary conditions are satisfied exactly and the method is robust, accurate, and particularly appropriate for complex geometry. The new approach is superior than the conventional Lagrangian (or Lagrangian–Eulerian) one for the geometrical quantities are handled by conservation laws (compatibility equations). Compared to any Eulerian method the new Lagrangian approach is characterized by the following features:

(1) A computational cell is literally a fluid particle and flow physics is closely followed. The computation is truly multi-dimensional, rather than the usual one-dimensional, splitting.

(2) A slip-surface is always crisply resolved without any detection and special treatment, since a computational cell remains identical to the same fluid particle all the time.

(3) The grid is automatically generated along the stream tubes as part of the solution. No a priori grid generation is needed.

(4) The inherent parallelism of the Lagrangian approach, that each computational cell may be considered as a fluid particle and a single processor interacting with its surrounding neighbours, lends itself to the simple implementation of massively parallel computation on machines such as the CM-2 to CM-5 models by the Thinking Machine Co. (this has been confirmed by the computations of the 2D version [19]).

In summary, the Lagrangian approach is observed to resolve both discontinuities (shocks and slip-surfaces) sharply in complicated geometry; once combined into massively parallel computation, we believe that it will become a powerful tool for steady supersonic flow computation. Research on the Lagrangian approach to transonic and subsonic inviscid compressible flows is currently underway and will be reported shortly.

APPENDIX: HYPERBOLICITY OF EQ. (13)

In this Appendix, we shall show that the Lagrangian conservation form (13) of the Euler equations is still of hyperbolic type provided the flow is supersonic everywhere. Let

$$\mathbf{Q} = (u, v, w, p, \rho, U, V, W, X, Y, Z)^{\mathrm{T}}.$$

The Lagrangian conservation form can be rewritten as

$$A_L \frac{\partial \mathbf{Q}}{\partial \lambda} + B_L \frac{\partial \mathbf{Q}}{\partial \xi} + C_L \frac{\partial \mathbf{Q}}{\partial \eta} = 0, \tag{A1}$$

where

$$A_L \frac{\partial \mathbf{E}}{\partial \mathbf{Q}} + B_L \frac{\partial \mathbf{F}}{\partial \mathbf{Q}} + C_L = \frac{\partial \mathbf{G}}{\partial \mathbf{Q}},$$

are 11×11 matrices (subscript "L" denotes Lagrangian):

$$A_L = \begin{bmatrix}
J_{11} & J_{12} & J_{13} & 0 & K/\rho^2 & 0 & 0 & 0 & 0 & 0 & 0 \\
0 & 0 & 0 & 1 & -a^2 & 0 & 0 & 0 & 0 & 0 & 0 \\
K & 0 & 0 & J_{11} & 0 & 0 & 0 & 0 & 0 & 0 & 0 \\
0 & K & 0 & J_{12} & 0 & 0 & 0 & 0 & 0 & 0 & 0 \\
0 & 0 & K & J_{13} & 0 & 0 & 0 & 0 & 0 & 0 & 0 \\
0 & 0 & 0 & 0 & 0 & 1 & 0 & 0 & 0 & 0 & 0 \\
0 & 0 & 0 & 0 & 0 & 0 & 1 & 0 & 0 & 0 & 0 \\
0 & 0 & 0 & 0 & 0 & 0 & 0 & 1 & 0 & 0 & 0 \\
0 & 0 & 0 & 0 & 0 & 0 & 0 & 0 & 1 & 0 & 0 \\
0 & 0 & 0 & 0 & 0 & 0 & 0 & 0 & 0 & 1 & 0 \\
0 & 0 & 0 & 0 & 0 & 0 & 0 & 0 & 0 & 0 & 1
\end{bmatrix},$$

$$B_L = \begin{bmatrix}
J_{21} & J_{22} & J_{23} & 0 & 0 & 0 & 0 & 0 & 0 & 0 & 0 \\
0 & 0 & 0 & 0 & 0 & 0 & 0 & 0 & 0 & 0 & 0 \\
0 & 0 & 0 & J_{21} & 0 & 0 & 0 & 0 & 0 & \frac{pw}{q} & \frac{-pv}{q} \\
0 & 0 & 0 & J_{22} & 0 & 0 & 0 & 0 & \frac{-pw}{q} & 0 & \frac{pu}{q} \\
0 & 0 & 0 & J_{23} & 0 & 0 & 0 & 0 & \frac{pv}{q} & \frac{-pu}{q} & 0 \\
\frac{(u^2/q^2-1)}{q} & \frac{uv}{q^3} & \frac{uw}{q^3} & 0 & 0 & 0 & 0 & 0 & 0 & 0 & 0 \\
\frac{uv}{q^3} & \frac{(v^2/q^2-1)}{q} & \frac{vw}{q^3} & 0 & 0 & 0 & 0 & 0 & 0 & 0 & 0 \\
\frac{uw}{q^3} & \frac{vw}{q^3} & \frac{(w^2/q^2-1)}{q} & 0 & 0 & 0 & 0 & 0 & 0 & 0 & 0 \\
0 & 0 & 0 & 0 & 0 & 0 & 0 & 0 & 0 & 0 & 0 \\
0 & 0 & 0 & 0 & 0 & 0 & 0 & 0 & 0 & 0 & 0 \\
0 & 0 & 0 & 0 & 0 & 0 & 0 & 0 & 0 & 0 & 0
\end{bmatrix},$$

$$C_L = \begin{bmatrix}
J_{31} & J_{32} & J_{33} & 0 & 0 & 0 & 0 & 0 & 0 & 0 & 0 \\
0 & 0 & 0 & 0 & 0 & 0 & 0 & 0 & 0 & 0 & 0 \\
0 & 0 & 0 & J_{31} & 0 & 0 & \frac{-pw}{q} & \frac{pv}{q} & 0 & 0 & 0 \\
0 & 0 & 0 & J_{32} & 0 & \frac{pw}{q} & 0 & \frac{-pu}{q} & 0 & 0 & 0 \\
0 & 0 & 0 & J_{33} & 0 & \frac{-pv}{q} & \frac{pu}{q} & 0 & 0 & 0 & 0 \\
0 & 0 & 0 & 0 & 0 & 0 & 0 & 0 & 0 & 0 & 0 \\
0 & 0 & 0 & 0 & 0 & 0 & 0 & 0 & 0 & 0 & 0 \\
0 & 0 & 0 & 0 & 0 & 0 & 0 & 0 & 0 & 0 & 0 \\
\frac{(u^2/q^2-1)}{q} & \frac{uv}{q^3} & \frac{uw}{q^3} & 0 & 0 & 0 & 0 & 0 & 0 & 0 & 0 \\
\frac{uv}{q^3} & \frac{(v^2/q^2-1)}{q} & 0 & 0 & 0 & 0 & 0 & 0 & 0 & 0 & 0 \\
\frac{uw}{q^3} & \frac{vw}{q^3} & \frac{(w^2/q^2-1)}{q} & 0 & 0 & 0 & 0 & 0 & 0 & 0 & 0
\end{bmatrix}.$$

The hyperbolicity of (A1), to be consistent with the commonly used one (for example, see Hirsch [20]), is defined as follows:

DEFINITION. The system (A1) is said to be hyperbolic, if all the eigenvalues μ

$$\det \|\mu A_L - \alpha B_L - \beta C_L\| = 0 \qquad \text{(A2)}$$

are real for any given real constants α and β ($\alpha^2 + \beta^2 \neq 0$).

By simple algebraic manipulation, the left-hand side of (A2) can be rewritten in a block diagonal form:

$$\begin{vmatrix} M & \mathbf{0} \\ \mathbf{0} & N \end{vmatrix},$$

where M is a 5×5 matrix,

$$M=\begin{vmatrix} \mu J_{11}-\alpha J_{21}-\beta J_{31} & \mu J_{12}-\alpha J_{22}-\beta J_{32} & \mu J_{13}-\alpha J_{23}-\beta J_{33} & 0 & \mu K/\rho^2 \\ 0 & 0 & 0 & \mu & -\mu a^2 \\ \mu K & 0 & 0 & \mu J_{11}-\alpha J_{21}-\beta J_{31} & 0 \\ 0 & \mu K & 0 & \mu J_{12}-\alpha J_{22}-\beta J_{32} & 0 \\ 0 & 0 & \mu K & \mu J_{13}-\alpha J_{23}-\beta J_{33} & 0 \end{vmatrix}$$

and N a 6×6 one,

$$N=\begin{vmatrix} \mu & 0 & 0 & 0 & 0 & 0 \\ 0 & \mu & 0 & 0 & 0 & 0 \\ 0 & 0 & \mu & 0 & 0 & 0 \\ 0 & 0 & 0 & \mu & 0 & 0 \\ 0 & 0 & 0 & 0 & \mu & 0 \\ 0 & 0 & 0 & 0 & 0 & \mu \end{vmatrix}.$$

The matrices M, N represent, respectively, the eigenequations from physical laws and geometrical laws (compatibility).

Since $\det\|N\|=\mu^6$, the geometrical laws, as expected, only involve a linearly degenerated mode with $\mu=0$. In the rest of the Appendix, we shall concentrate to show that all the roots of $\det\|M\|=0$ are real if the flow is supersonic everywhere. Thus the system (A1) and hence (13) is of hyperbolic type.

To find the roots of $\det\|M\|=0$, we first note that M only involves the upper left corner 5×5 submatrices of A_L, B_L, and C_L, namely, A_l, B_l and C_l,

$$A_l=\begin{pmatrix} J_{11} & J_{12} & J_{13} & 0 & K/\rho^2 \\ 0 & 0 & 0 & 1 & -a^2 \\ K & 0 & 0 & J_{11} & 0 \\ 0 & K & 0 & J_{12} & 0 \\ 0 & 0 & K & J_{13} & 0 \end{pmatrix},$$

$$B_l=\begin{pmatrix} J_{21} & J_{22} & J_{23} & 0 & 0 \\ 0 & 0 & 0 & 0 & 0 \\ 0 & 0 & 0 & J_{21} & 0 \\ 0 & 0 & 0 & J_{22} & 0 \\ 0 & 0 & 0 & J_{23} & 0 \end{pmatrix},$$

$$C_l=\begin{pmatrix} J_{31} & J_{32} & J_{33} & 0 & 0 \\ 0 & 0 & 0 & 0 & 0 \\ 0 & 0 & 0 & J_{31} & 0 \\ 0 & 0 & 0 & J_{32} & 0 \\ 0 & 0 & 0 & J_{33} & 0 \end{pmatrix},$$

and $\det\|M\|=0$ has the form

$$\det\|\mu A_l-\alpha B_l-\beta C_l\|=0. \tag{A3}$$

This can be shown to be associated with the Euler equations in Lagrangian variables,

$$A_l\frac{\partial \mathbf{Q}'}{\partial\lambda}+B_l\frac{\partial \mathbf{Q}'}{\partial\xi}+C_l\frac{\partial \mathbf{Q}'}{\partial\eta}=0, \tag{A4}$$

where $\mathbf{Q}'=(u, v, w, p, \rho)^{\mathrm{T}}$.

We also note that (A4) can be derived directly from the Euler equations of (1) by the coordinate transformation between (x, y, z) and (λ, ξ, η). The details are illustrated as follows:

Similar to (13), the Euler equations (1) can be rewritten in the form of (A1),

$$A_E\frac{\partial \mathbf{Q}'}{\partial x}+B_E\frac{\partial \mathbf{Q}'}{\partial y}+C_E\frac{\partial \mathbf{Q}'}{\partial z}=0, \tag{A5}$$

where the subscript "E" represents Eulerian. The hyperbolicity of (A5) stipulates (see, for example, [20]) that for any given real constants α' and β' $(\alpha'^2+\beta'^2\neq 0)$, the eigenequation

$$\det\|\mu' A_E-\alpha' B_E-\beta' C_E\|=0 \tag{A6}$$

always has real roots μ' (eigenvalues).

Recall that

$$\frac{\partial}{\partial\lambda}=\left(j_{11}\frac{\partial}{\partial x}+j_{12}\frac{\partial}{\partial y}+j_{13}\frac{\partial}{\partial z}\right),$$

$$\frac{\partial}{\partial\xi}=\left(j_{21}\frac{\partial}{\partial x}+j_{22}\frac{\partial}{\partial y}+j_{23}\frac{\partial}{\partial z}\right),$$

$$\frac{\partial}{\partial\eta}=\left(j_{31}\frac{\partial}{\partial x}+j_{32}\frac{\partial}{\partial y}+j_{33}\frac{\partial}{\partial z}\right),$$

where j_{rs} $(r, s=1, 2, 3)$ are the elements of the Jacobian

$$J_0=\frac{\partial(x, y, z)}{\partial(\lambda, \xi, \eta)}.$$

Substituting these into (A4) and collecting like terms, we have a form of (A5),

$$(j_{11}A_l+j_{21}B_l+j_{31}C_l)\frac{\partial \mathbf{Q}'}{\partial x}+(j_{12}A_l+j_{22}B_l+j_{32}C_l)\frac{\partial \mathbf{Q}'}{\partial y}$$

$$+(j_{13}A_l+j_{23}B_l+j_{33}C_l)\frac{\partial \mathbf{Q}'}{\partial z}=0. \tag{A7}$$

It is well known that if the flow is supersonic everywhere, the Euler equation (A5) or (A7) is of hyperbolic type. From the hyperbolicity of (A7), the eigenequation (A6)

$$\det \|\mu'(j_{11}A_l + j_{21}B_l + j_{31}C_l) - \alpha'(j_{12}A_l + j_{22}B_l + j_{32}C_l) - \beta'(j_{13}A_l + j_{23}B_l + j_{33}C_l)\| = 0 \tag{A8}$$

has real roots μ' for any given constants α' and β'. By rearranging terms in (A8), we have a form of (A3), i.e., $\det \|M\| = 0$,

$$\det \|(\mu' j_{11} - \alpha' j_{12} - \beta' j_{13})\, A_l + (\mu' j_{21} - \alpha' j_{22} - \beta' j_{23})\, B_l + (\mu' j_{31} - \alpha' j_{32} - \beta' j_{33})\, C_l\| = 0. \tag{A9}$$

Comparing (A9) with (A3), it is observed that there exists a one-to-one correspondence between (μ, α, β) and (μ', α', β') $(|J_0| \neq 0)$ and that (μ, α, β) can be regarded as the linear combination of (μ', α', β'). Since no complex number is involved in the operation, we conclude that all the eigenvalues μ for $\det \|M\| = 0$ must be real and that the system (A1) or (13) is of hyperbolic type. As a matter of fact, it can be shown that for (A1) there are two non-zero real eigenvalues corresponding to the Mach concoid characteristic directions and one eigenvalue of $\mu = 0$ with multiplicity of nine, corresponding to the stream direction.

REFERENCES

1. P. L. Roe, *Lecture Notes in Physics*, Vol. 23 (Springer-Verlag, New York/Berlin, 1991), p. 69.
2. W. Hermann and L. D. Bertholf, in *Computational Methods for Transient Analysis*, edited by T. Belytschko and T. J. R. Hughes (North-Holland, Amsterdam, 1983), Chap. 8.
3. A. Harten, *J. Comput. Phys.* **83**, 148 (1989).
4. C. Y. Loh and W. H. Hui, *J. Comput. Phys.* **89**, 207 (1990).
5. W. H. Hui and H. Van Roessel, in *Proceedings, NATO AGARD Symposium on Unsteady Aerodynamics—Fundamentals and Application to Aircraft Dynamics, Göttingen, West Germany, 1985*, S1, CP-386.
6. C. Y. Loh and W. H. Hui, AIAA Paper 89-1963-CP, 1989 (unpublished).
7. W. H. Hui and Y. C. Zhao, in *Proceedings, 4th International Conference on Hyperbolic Problems*, edited by A. Donato and F. Oliveri, Notes on Numerical Fluid Mechanics, (Vieweg, Wiesbaden, 1993).
8. P. K. Sweby, *SIAM J. Numer. Anal.* **21**, 995 (1984).
9. S. K. Godunov, *Mat. Sb.* **47**, 271 (1959).
10. T. Chang and Y. Zheng, *SIAM J. Math. Anal.* **21**, 593 (1990).
11. A. Harten, J. M. Hyman, and P. D. Lax, *Commun. Pure Appl. Math.* **29**, 297 (1976).
12. M. G. Crandall and A. Majda, *Math. Comput.* **34**, 1 (1980).
13. W. H. Hui and C. Y. Loh, *J. Comput. Phys.* **103**, 450 (1992).
14. R. Courant and D. Hilbert, *Methods of Mathematical Physics, Part II* (Academic Press, New York/London, 1962).
15. W. H. Hui and C. Y. Loh, *J. Comput. Phys.* **103**, 465 (1992).
16. F. Marconi and G. Moretti, AIAA Paper 76-383, 1976 (unpublished).
17. J. E. West and R. H. Korkegi, *AIAA J.* **10**, 652 (1972).
18. M. S. Liou and A. T. Hsu, AIAA Paper 89-1994-CP, 1989 (unpublished).
19. M.-F. Liou and C. Y. Loh, NASA TM-104446, 1991; also in *Parallel Comput. Fluid Dynamics, Stuggart, Germany, 1991*, edited by K. G. Reinsch *et al.*, (North-Holland, Amsterdam, 1992).
20. C. Hirsch, *Numerical Computation of Internal and External Flows*, Vol. 2 (Wiley, New York, 1989).